Co-planar grid and Frisch-ring CdZnTe detectors: intrinsic and material related performance limitations

Gabriella Carini

Department of Electrical Engineering (DIEPA), University of Palermo, Italy

Detector Development and Testing Division,
Nonproliferation and National Security Department, BNL

A. Bolotnikov, G. Camarda, G. De Geronimo, P. Siddons, G. Wright, and R. James

BROOKHAVEN NATIONAL LABORATORY

Università degli Studi di Palermo

Outline

- Introduction: CdZnTe and gamma-ray detectors
- Frisch grid: the idea behind co-planar grid and …
- … Frisch-ring detectors
- Material defects: current limitation
- Conclusions

Cadmium Zinc Telluride

Cadmium Zinc Telluride $Cd_{1-x}Zn_xTe$

II-VI compound semiconductor

x = 0.10 for grade detector material

E_{gap} = 1.6 eV

Z =48,30,52

$\rho = (1.0 \div 9.0) \times 10^{10}\ \Omega$ cm

$\mu_e \tau_e = (3 \div 10.0) \times 10^{-3}\ cm^2/V$ $\mu_h \tau_h \approx (2 \div 5) \times 10^{-5}\ cm^2/V$

Cadmium Zinc Telluride

Semi-conductor	E_{gap} [eV]	μ_h / μ_e [cm^2/Vs]	ρ [Ω cm]	Density [g/cm^3]	Z	ε [eV]
Si	1.12	480 1350	2.3×10^5	2.33	14	3.6
Ge	0.67	1900 3900	47	5.33	32	2.9
CdTe	1.44	100 1100	1×10^9	5.85	48,52	4.43
CdZnTe	1.6	100 1000	5×10^{11}	5.81	48,30,52	4.7

Crystals…

macrodomains

grain boundaries decorated
with tellurium inclusions

twin boundaries

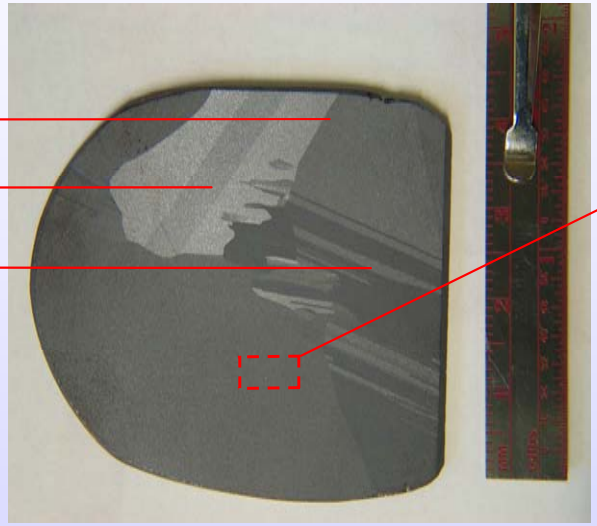

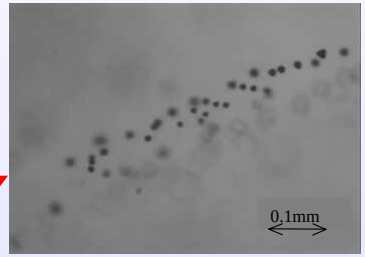

tellurium inclusions

CZT slice and an IR transmission image

CdZnTe advantages and limitations

- Wide Band Gap → Room Temperature.
- High Atomic Number + High density → High Stopping Power.
- High Resistivity → Low Leakage Current.
- Electron Transport Properties → $\mu_e \tau_e \approx 5*10^{-3}$ cm^2/V.
- Crystal Quality → Material Nonuniformities.
- Poor Hole Transport Properties → $\mu_h \tau_h \approx 10^{-5}$ cm^2/V.

Hard X-ray and γ-ray detectors

…To resume CdZnTe is an attractive material for the fabrication of high-energy detectors. Its large band-gap allows to operate at room temperature and the high atomic numbers of the elements composing the material give a high quantum efficiency.

• In principle detectors are simple devices that directly convert charges generated by ionizing radiation, such as X-rays, Gamma rays, and Beta particles, into electrical signals.

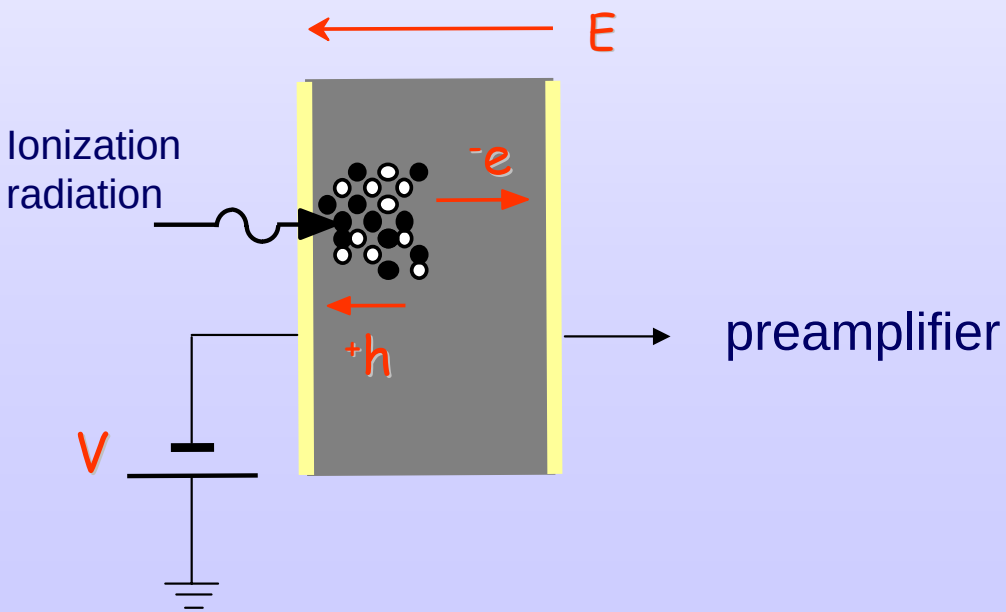

Applications

- Isotopes identification for homeland security.

- Medical: is replacing the old scintillator based detector. E.g. Bone Mineral Densitometry, Gamma Probe, Nuclear Medicine.

- Astronomy: NASA's SWIFT to measure gamma ray bursts was launched last November.

CPG & Frisch-ring detectors

Application: as a gamma ray spectrometer.

Frisch-ring: it produces very good energy resolution with the least expensive material. It gives imaging capability.

Simple read-out: both can be used without customized electronics.

Potentially High efficiency.

CPG higher active volume device.

Coplanar-grid study: Motivations

Coplanar grid gamma-ray detectors have demonstrated good spectral performance on CZT material. Good detectors provides an energy resolution < 2% @ 662 keV.

Several factors can degrade the performance of coplanar-grid devices: contacts geometry, electron trapping, material non-uniformity, surface and edge effects, charge sharing, electronic noise, etc.

In this part of the talk, we concentrated on the studies of the intrinsic effects related to the coplanar-grid contact configuration and how electron trapping and electric field variations can magnify these effects.

The idea behind CoPlanar Grids

FRISCH GRID

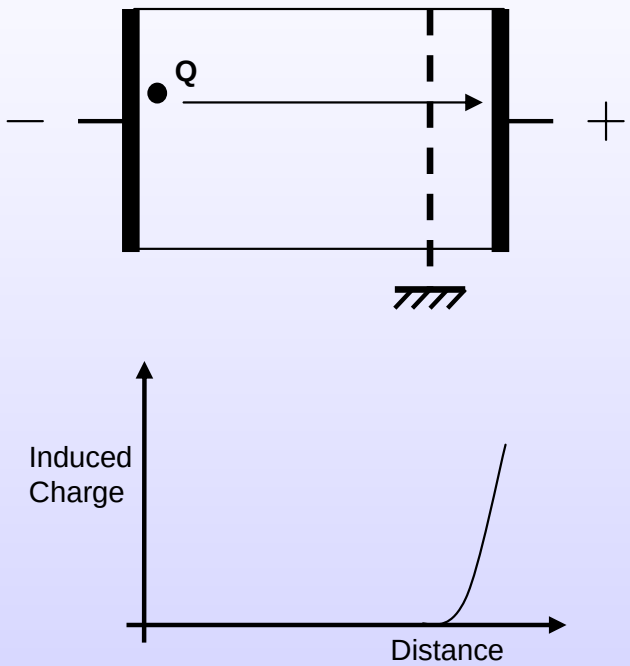

Induced charge at the anode vs distance traveled by the charge Q

COPLANAR GRIDS*

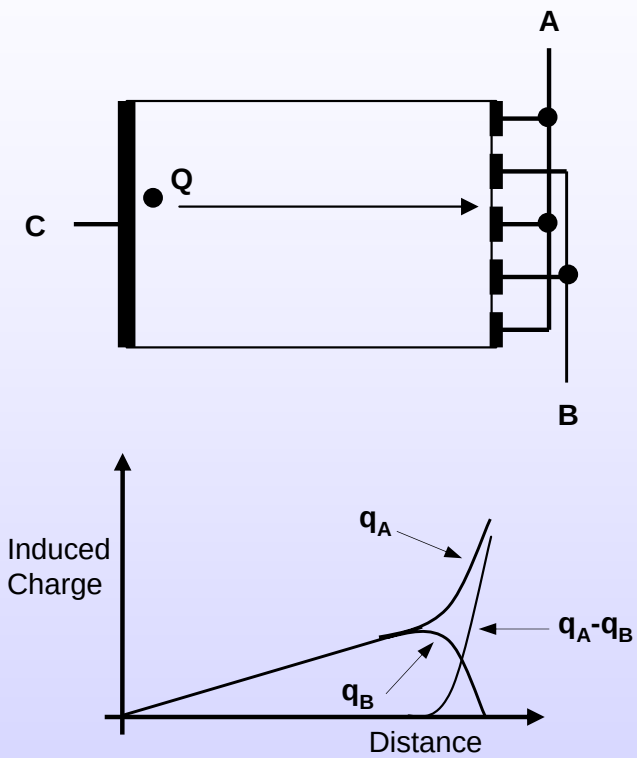

Induced charge at the electrodes (A and B) and the difference signal vs distance traveled by the charge Q which is collected at electrode A

* P. Luke, APL 28 November 1994

CoPlanar Grid vs Planar

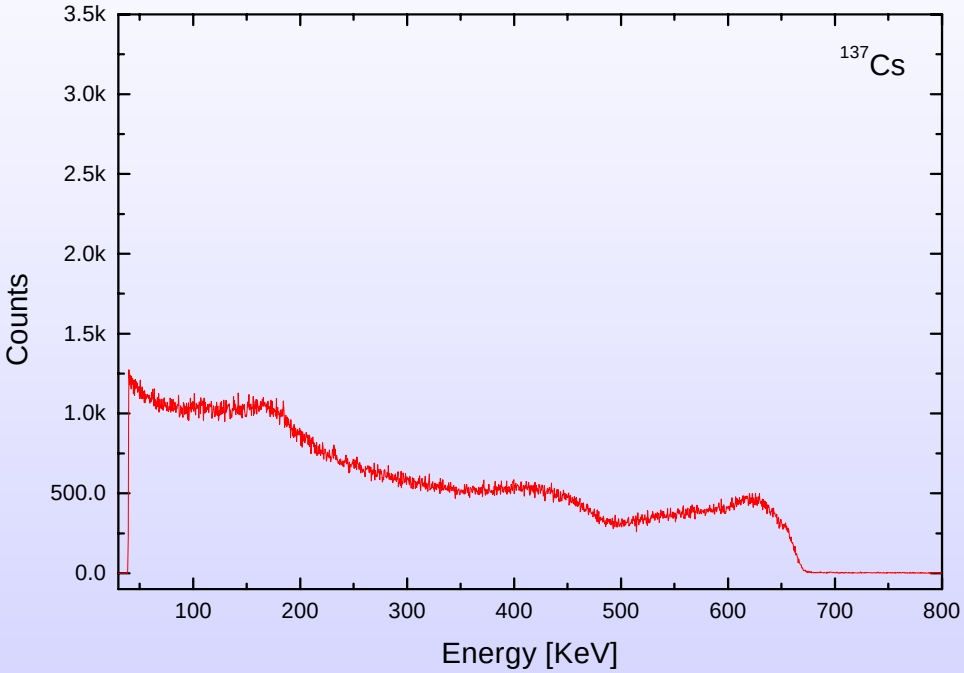

Spectrum of ^{137}Cs obtained with the CZT detector in a standard **PLANAR** configuration.

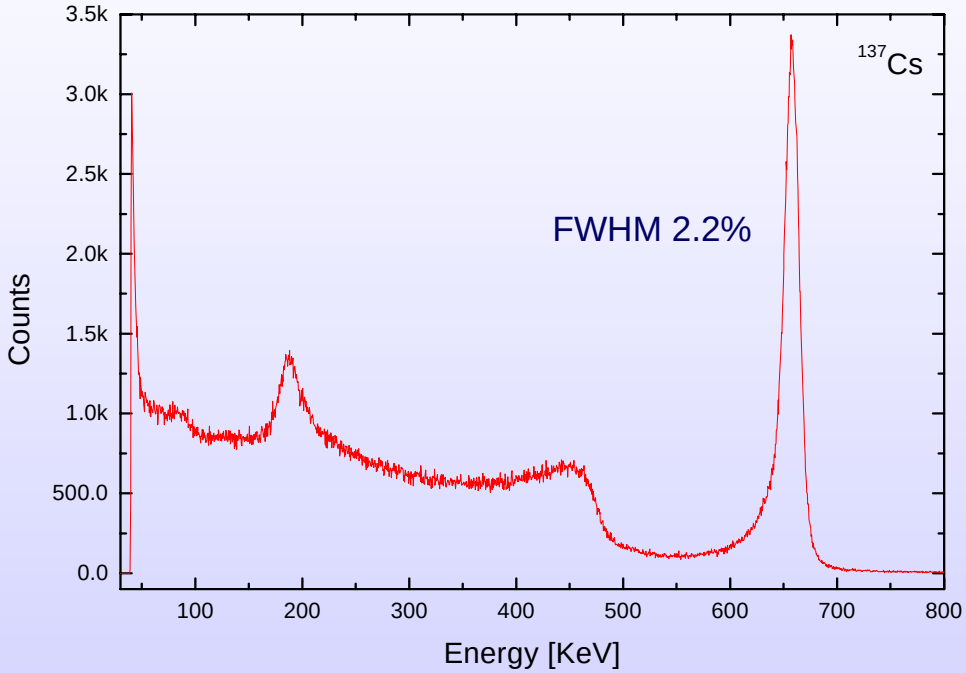

Spectrum of ^{137}Cs obtained with the CZT detector using the **COPLANAR GRID** technique.

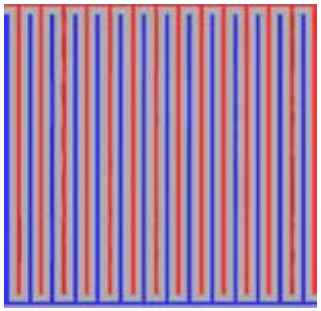

CoPlanar Grid principle

The idea of a coplanar-grid device is based on the symmetrical responses of the collecting and non-collecting grids.

The device's output signal for the idealized case is proportional to the total collected charge and it is independent of locations of interaction points:

$$A_{out}=A_{col}-A_{non}=(Q_{col}+Q'_{col})-Q'_{non}=Q_{col}$$

where Q_{col} is the total collected charge, and Q'_{col} and Q'_{non} are the charge signals induced on the collecting and non-collecting grids by holes and trapped electrons.

The difference $Q'_{col}-Q'_{non}$ is not negligible in the real CPG device and depends on the location of the interaction point. Moreover, the collected charge Q_{col} also depends on the position of interaction point due to the electron trapping in the device volume.

These effects degrade the spectroscopic response of the CPG detectors.

Waveforms analysis

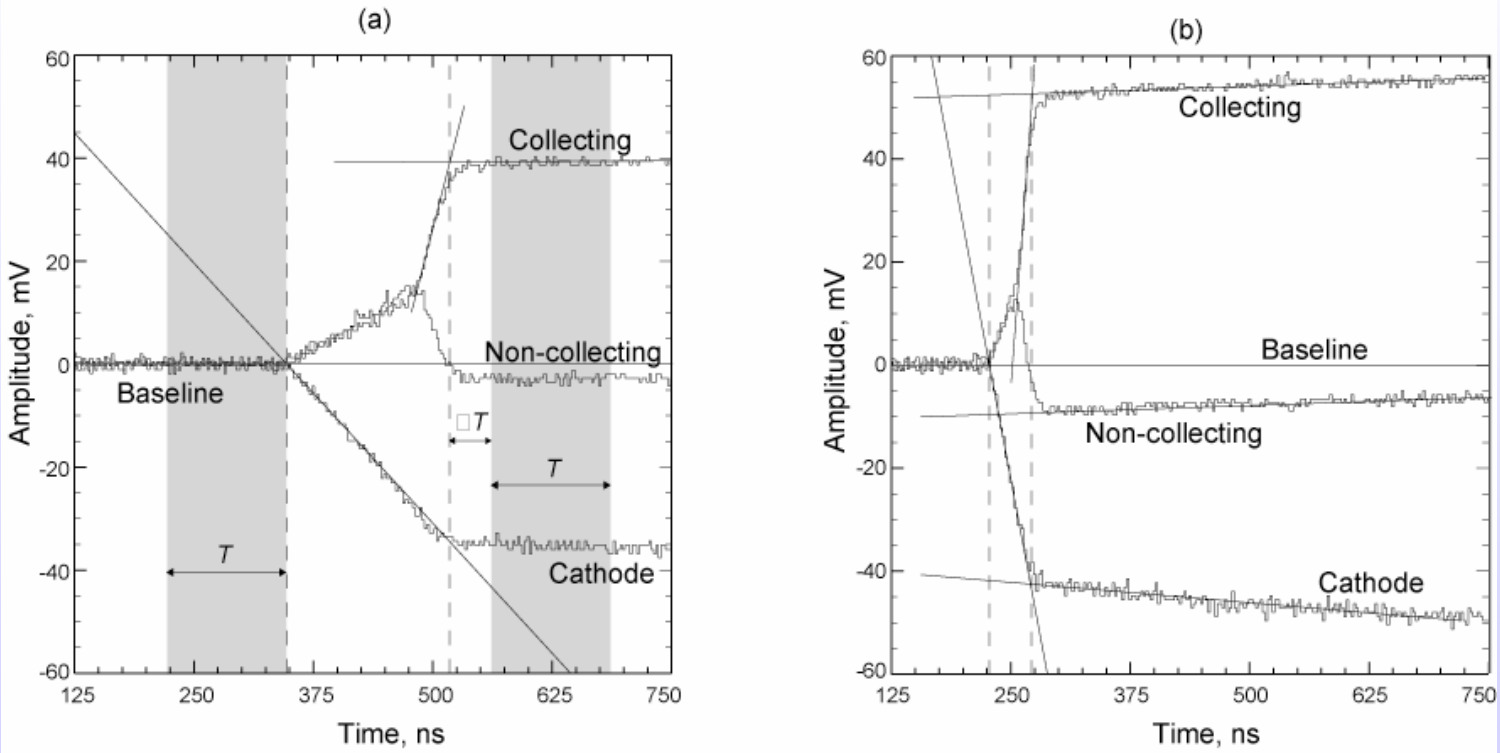

Correlation plots

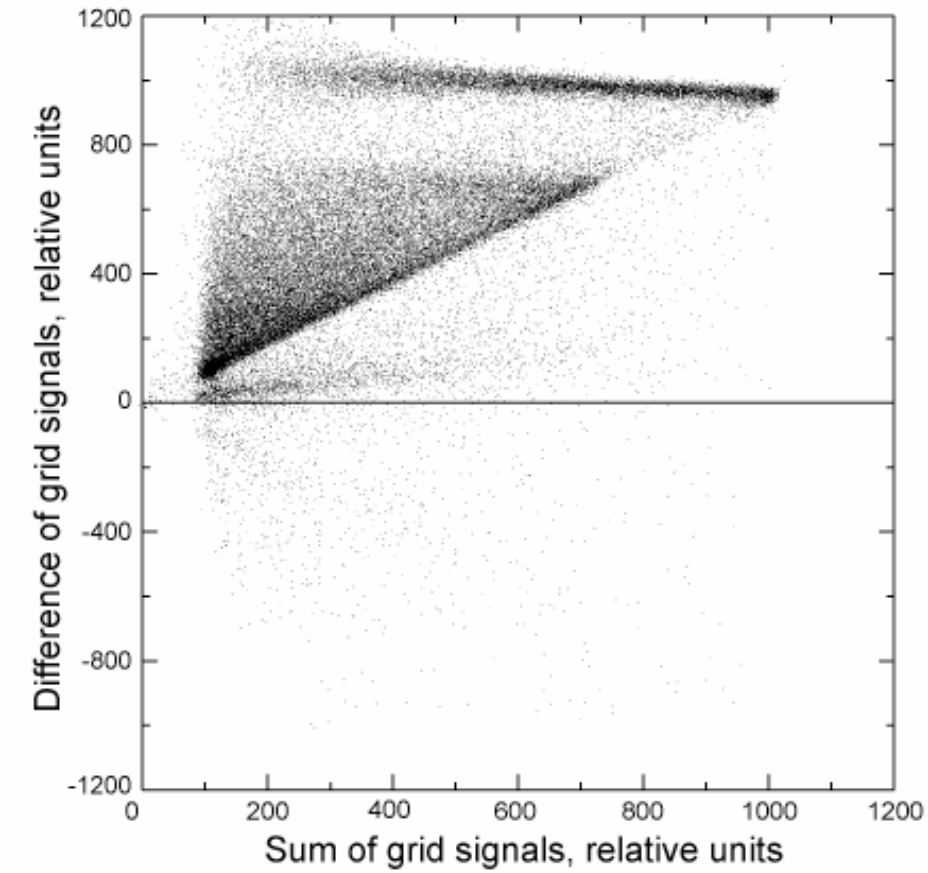

First, the tracks of the dots, corresponding to the total energy absorption events, bend off the lines $|A_1-A_2|=Q_0$, which indicates the charge loss in CZT bulk due to electron trapping. The actual tracks location follows the line $|A_1-aA_2|=Q_0$, where a is a numerical coefficient, independent of the photon energy.

Second, the dots distribution broadening indicates the *global* asymmetry between the grids weighting potentials. It is well known that these areas are located near the device's edges. This effect results in the long tails usually seen on the right and left wings of the peaks in the pulse-height spectra measured for CPG devices.

Third, the width of the dots distribution in the track above the threshold where it starts broadening can be explained by the electronic noise in the grids' signals and by the *local* variations in the grids' signals. This is caused by the *local* dependences of the collected charge and grids weighting potentials.

X12A Beamline Setup

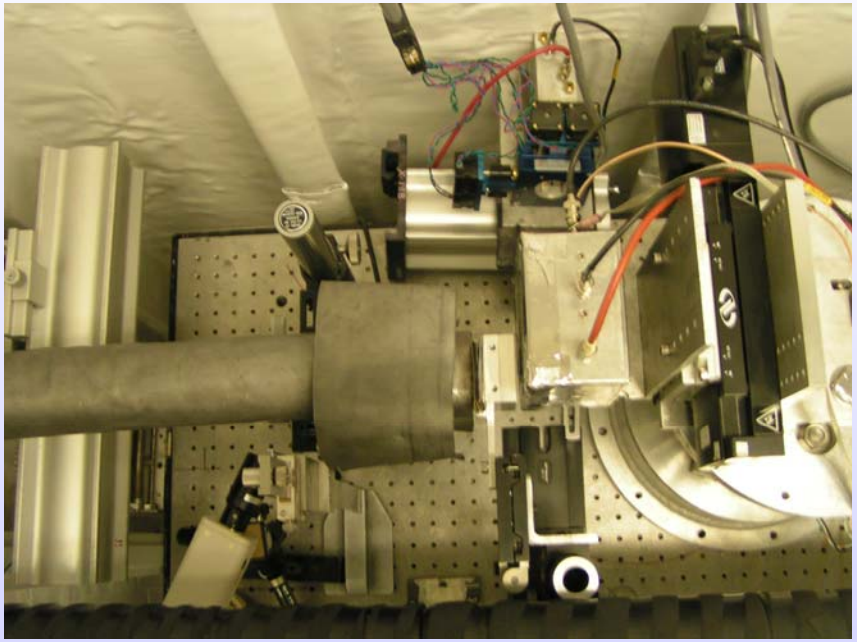

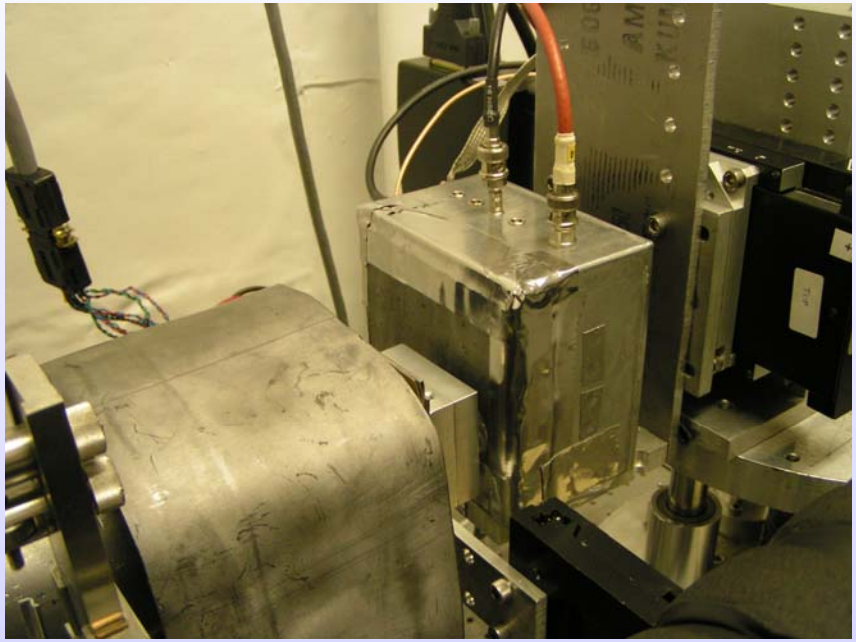

Data collection trough MCA and digital scope

X12A Measurement parameters

- The detector was irradiated from the cathode
- White beam mode (1-100keV) with attenuator
- Beam Energy ~ 85keV
- Beam Size 25μm x 25μm / 10μm x 10μm
- Pixel size < 100μm x 100μm
- Time of collection per point: 1-3s
- 15×15×7 mm^3 CPG detectors from eV-Products were used to take most of the measurements showed.

MCA calibration

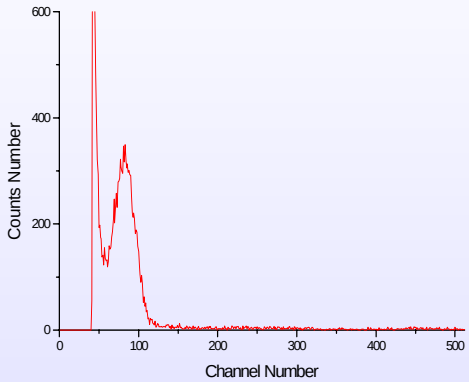

^{241}Am spectrum

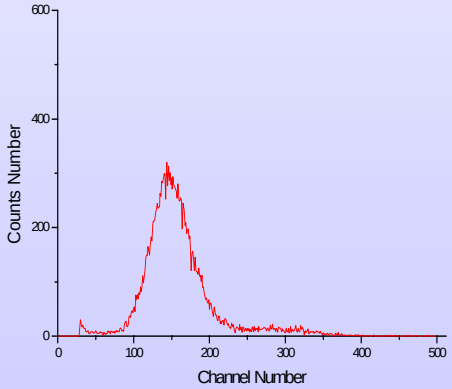

Beam spectrum

X12A Data collection

Two types of data

- Energy pulses through the MCA

- Waveforms trough the SCOPE

From the first set:

- Analysis of Peak position, FWHM, Amplitude resulting from Gaussian fitting.

From the second set:

- Pulses processing on hundreds of waveforms.

Block diagram of the ASIC for CPG*

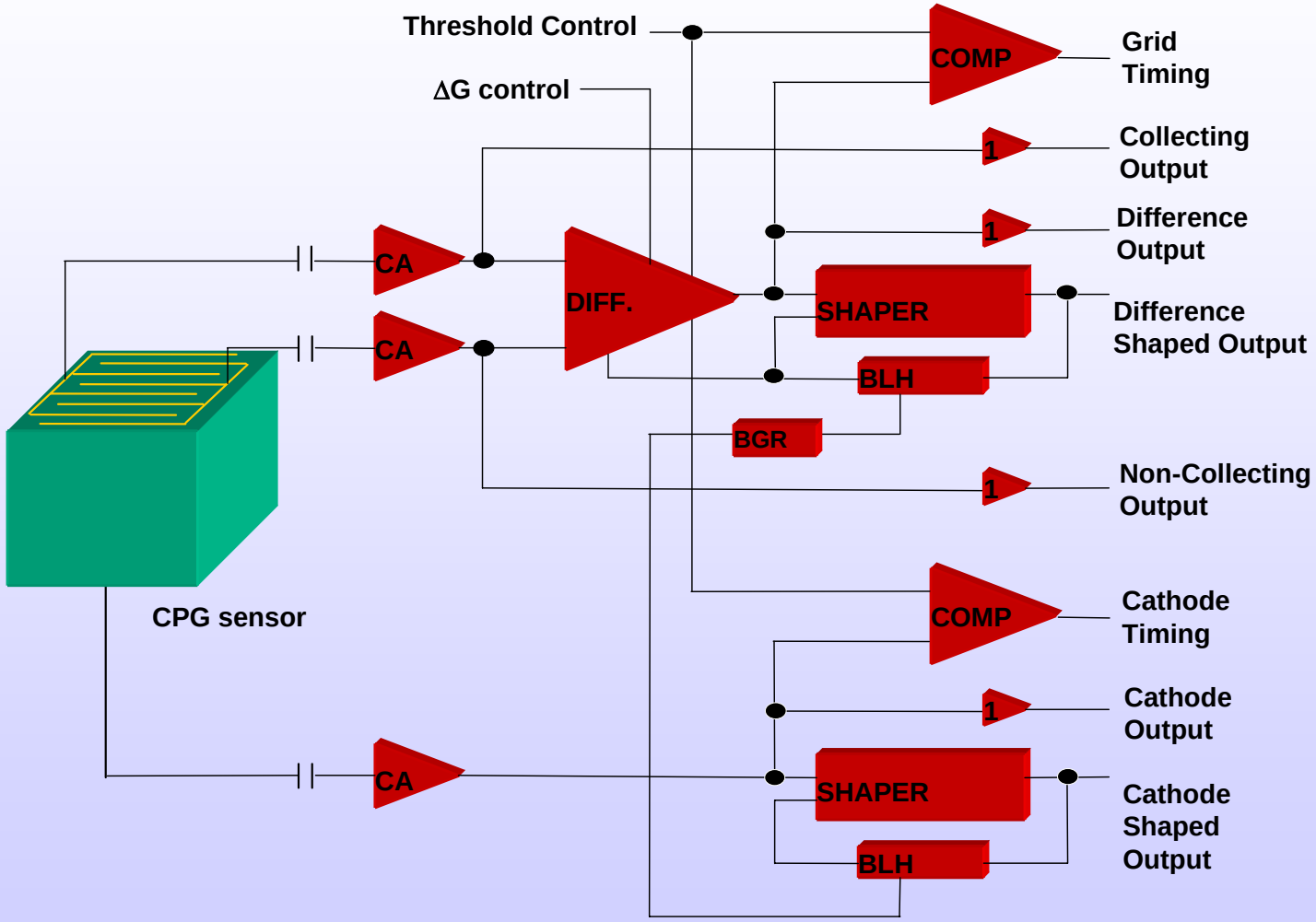

* Gianluigi De Geronimo

Some scan maps

Difference
peak to peak
in the “uniform”
area ~1.6%

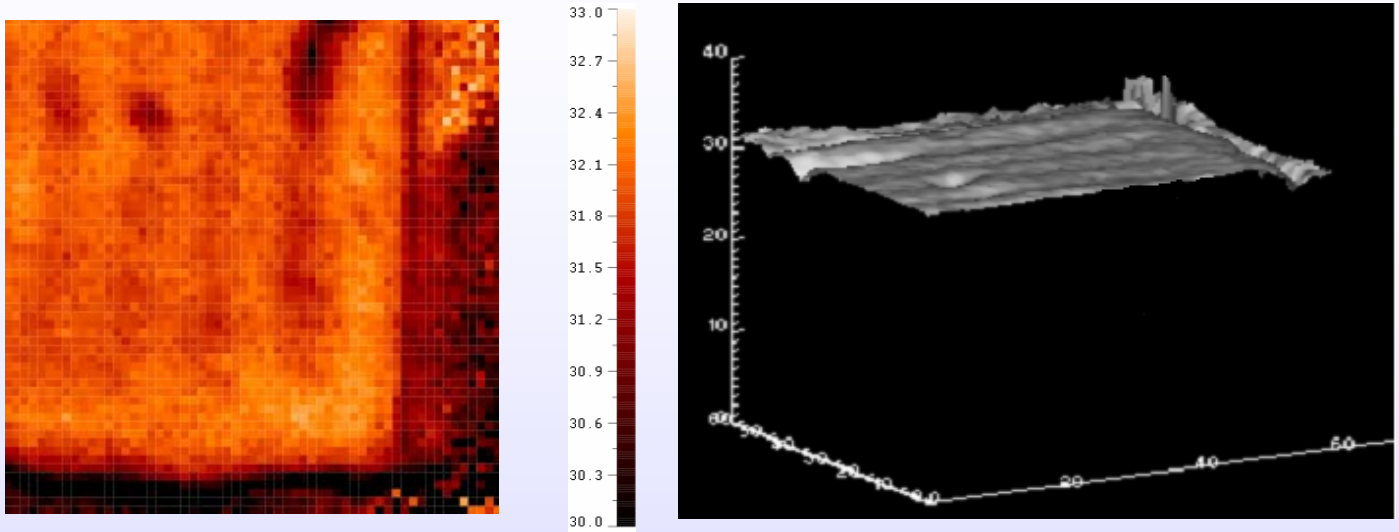

Strong variations of the detector responses that correlate directly with the contact patterns of the devices are shown above.

The amplitudes of the output signals diminish when the X-ray beam is pointed above the areas of the non-collecting strips.

These reductions in amplitudes, which fluctuate over the detector area, affect the energy resolution of the device.

Some scan maps

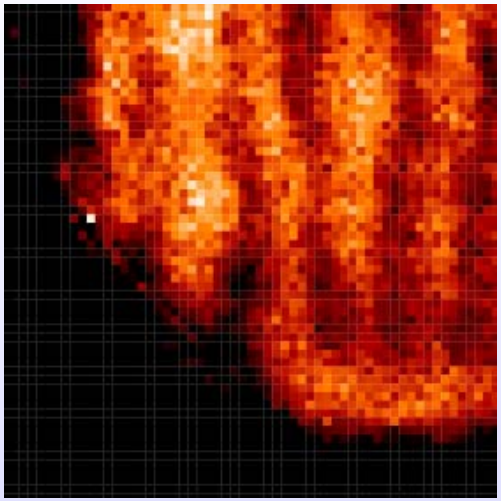

Wires for the connections were glued using silver print.
Scan of a corner with the contact.

Some scan maps

a) Peak Position vs (x,z) position
b) FWHM vs (x,z) position

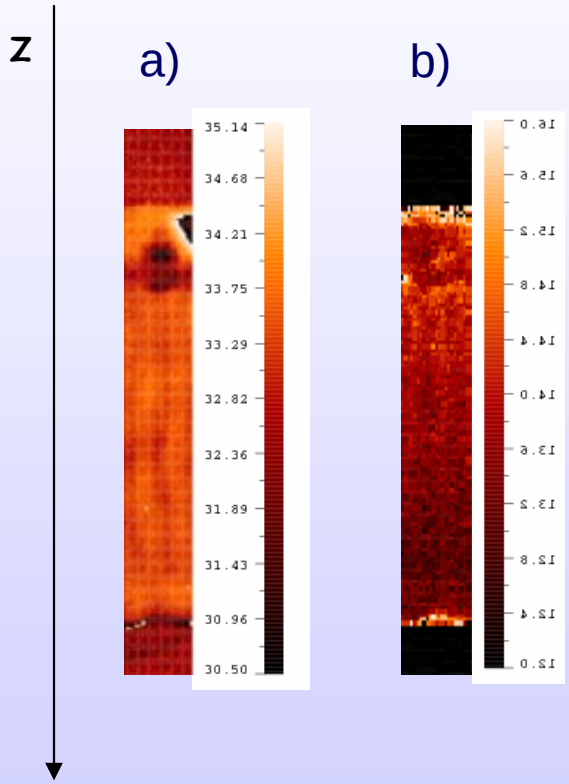

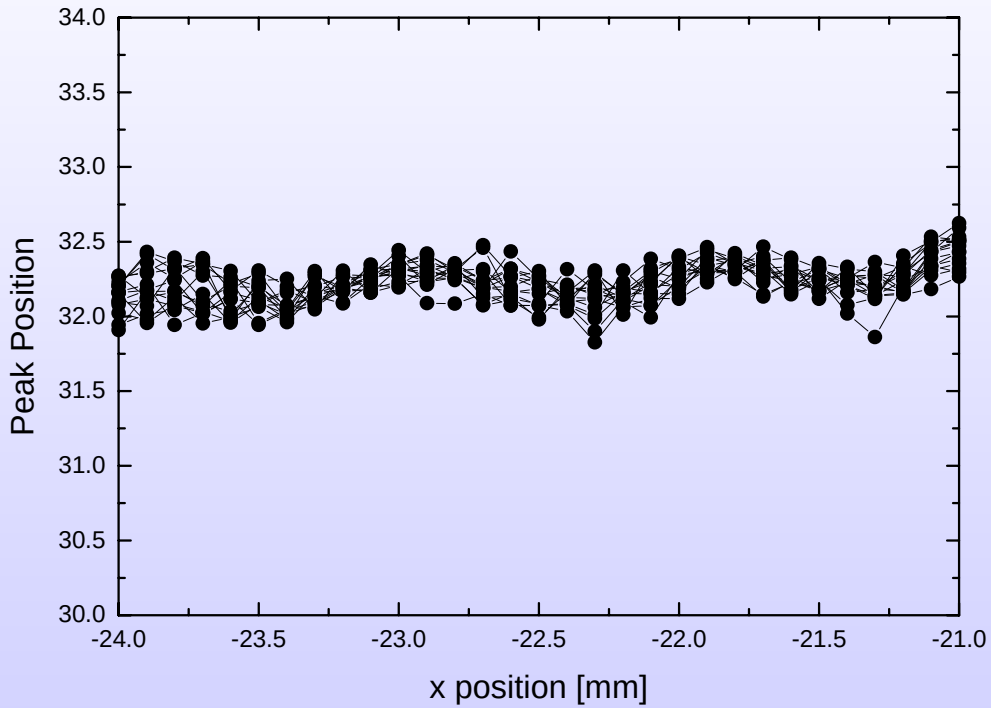

Cross section

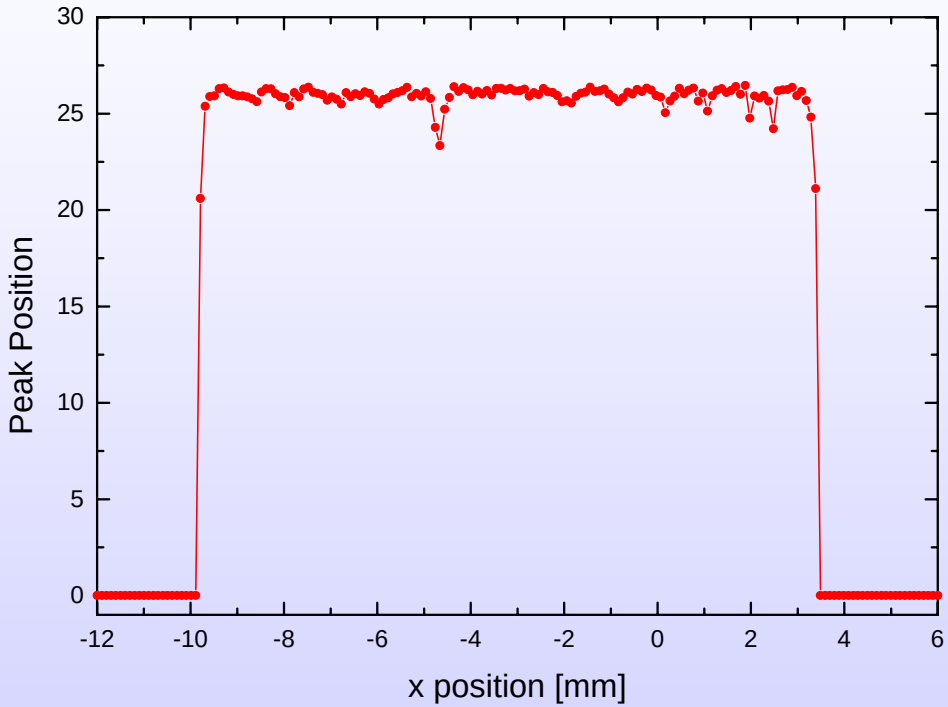

V_K=-600V V_G=-45V

Step= 100μm Beam= 25μm x 25μm

Scans at different bias values

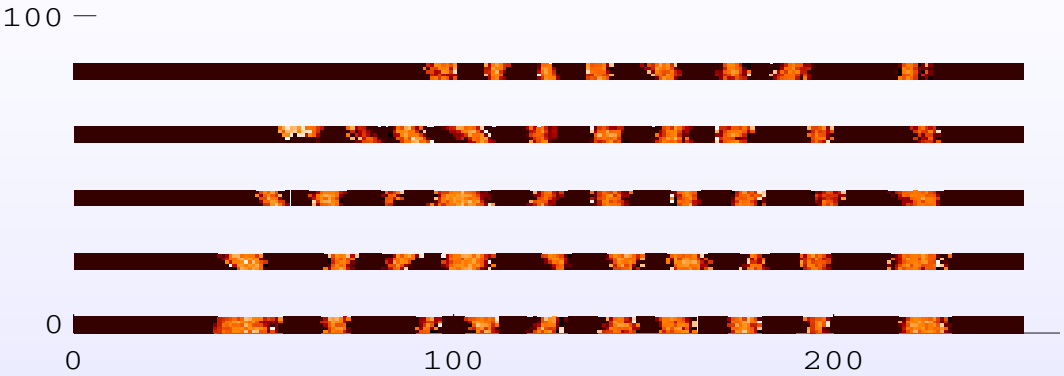

V_k=-1000V; V_G=0V

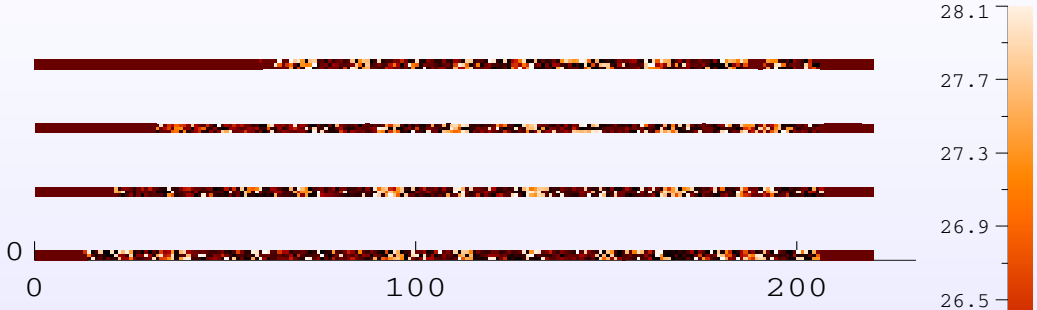

V_k=-800V; V_G=-24V

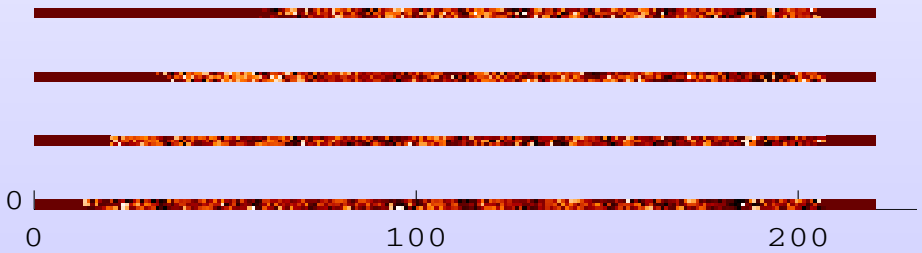

V_k=-1000V; V_G=-30V

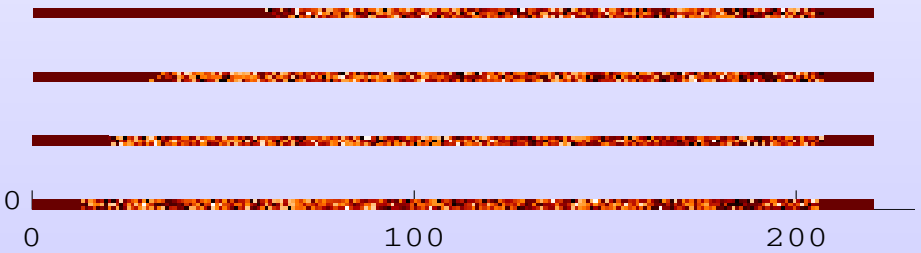

V_k=-1200V; V_G=-36V

Cross sections of two different sensors

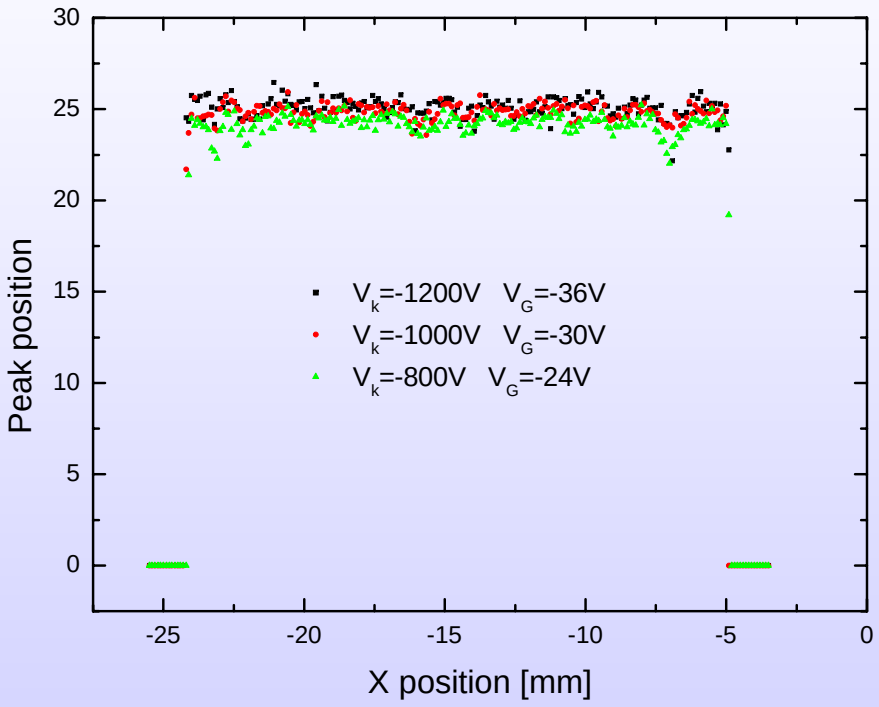

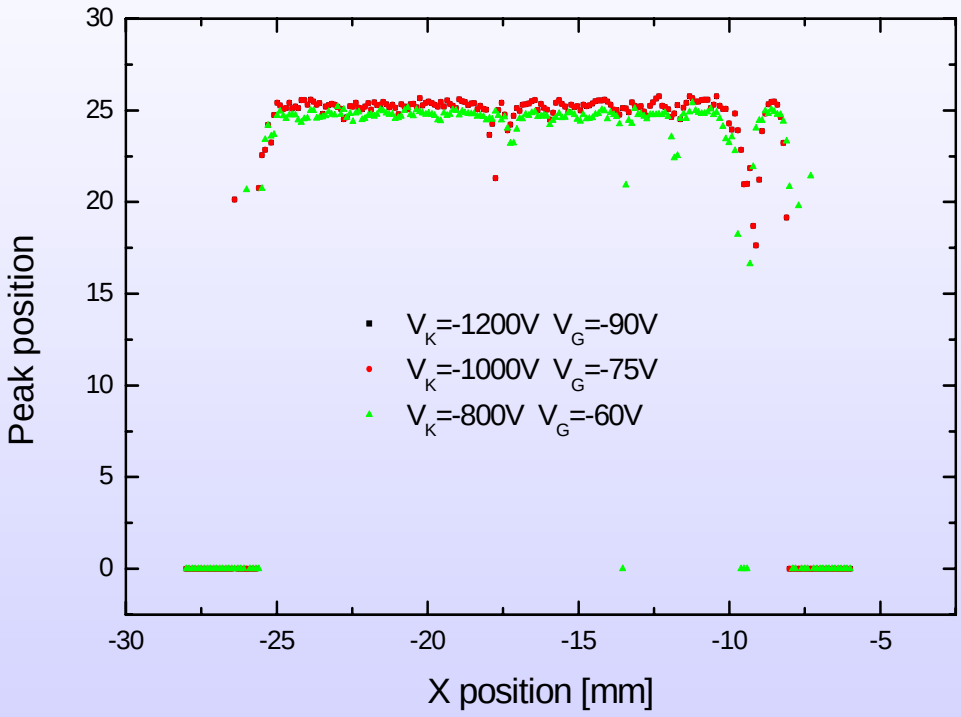

Dependences of $(A_{col}-A_{non})/(A_{col}+A_{non})$ vs. the beam position measured at several differential biases values between the grids

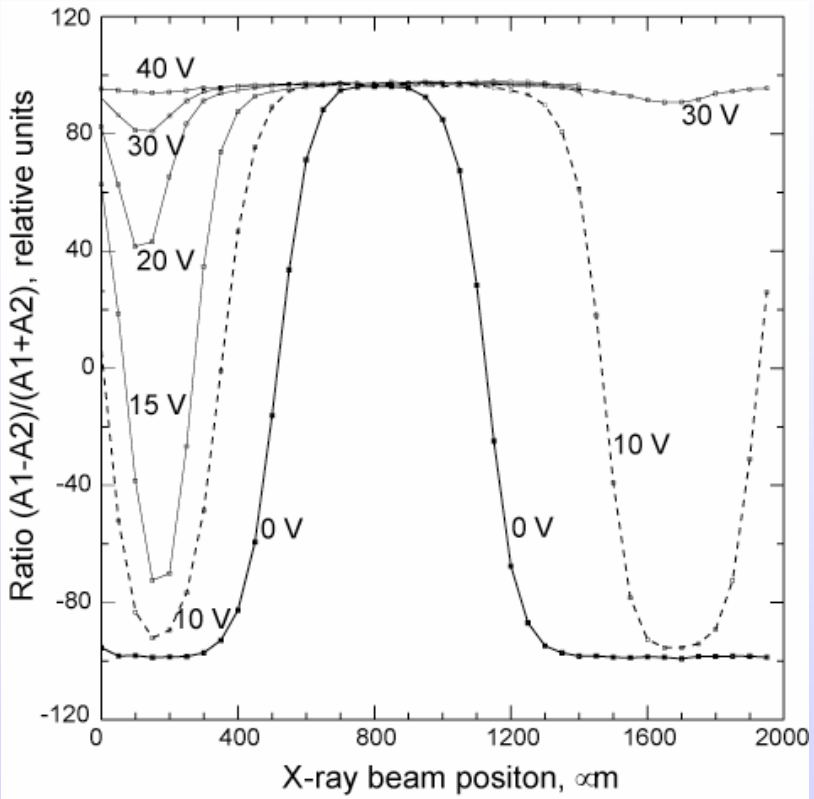

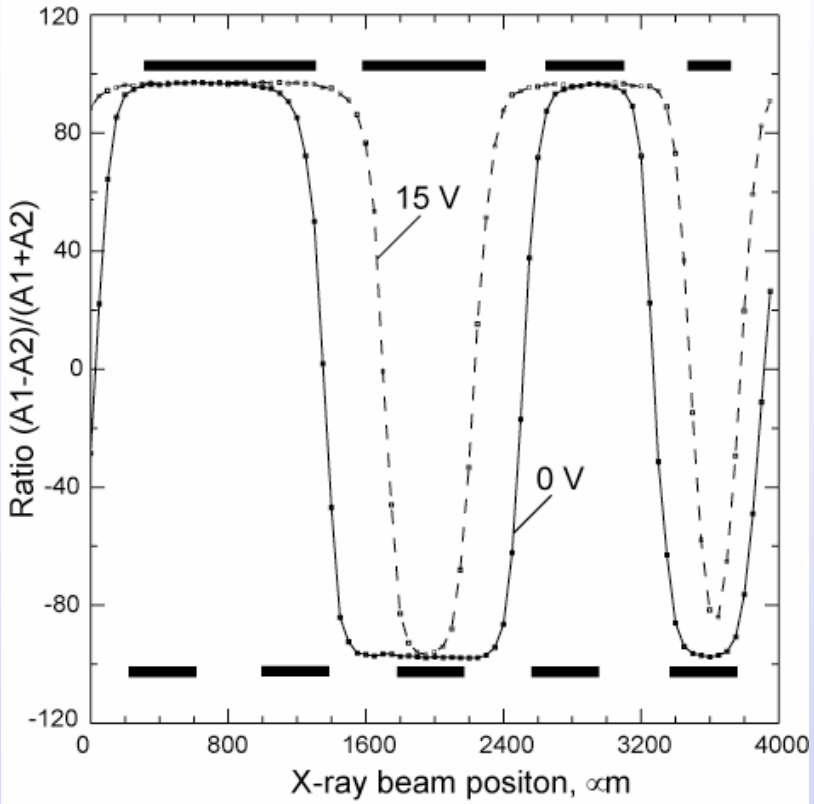

The device response becomes almost flat (saturated) at the differential grid bias of 40V, which is about 2.5 times smaller than the value calculated for the same device geometry under the assumption of no space charge inside the crystal.

Discussion

The electric field inside the detector is not uniform in both the vertical and horizontal directions.

The average electric-field strength decreases toward the anode (as if space charge existed inside the detector), resulting in a smaller differential grid bias required to steer all the electrons toward the collecting strips. At the same time, the lateral field variations cause random changes in the apparent strip locations in the x-ray map.

Discussion

Three effects can be responsible for the observed variations.

❖The first is related to the different length of the passes traveled by the electron clouds from the points of interactions to the collecting grid. The smaller amount of charge is lost when the interaction point is located above the collecting strip (the straight path) and the larger charge loss occurs when the path originates above the non-collecting strip (the curved path).

❖Second, the *local* dependences of the grids weighting potentials are anti-correlated (i.e., the stronger signal is induced on the grid whose strip is closer to the interaction point). As a result, the *local* variations of the signals induced by the uncollected charges (both the holes and trapped electrons) add up when the grids' signals are subtracted.

❖ Third effect is the charge loss at the surface between the strips.

Discussion

Even at high differential bias between the grids the field lines originated at the cathode intersect the surface between the strips. Hence, the electrons can reach the surface which has different electronic properties than CdZnTe bulk. The electron mobility at the surface is less while the concentration of the traps is high. As a result, some fraction of the charge is lost in the gaps between the strips, which gives variations in the device response. In fact CdZnTe is very sensitive to surface effects and surface properties strongly influence detector performances. Similar effect was reported by others.

Field distribution

7 mm thick coplanar-grid CZT
Pitch 250 um
Cathode bias -1000 V

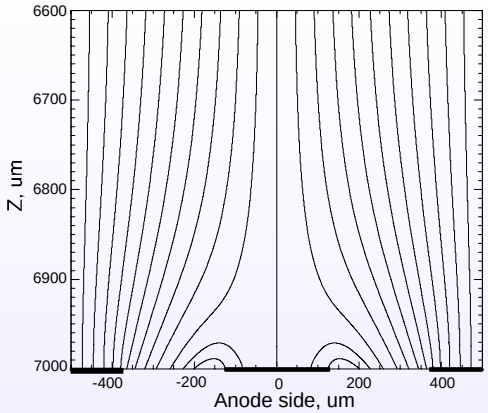

Differential bias –50V

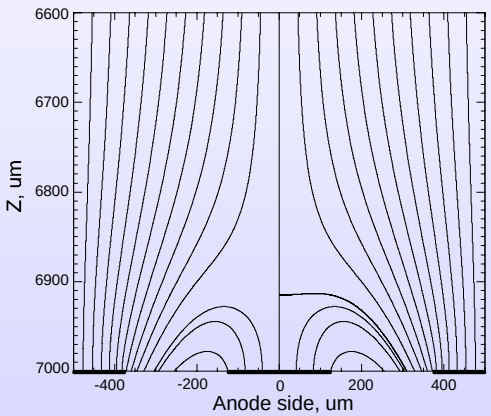

Differential bias –75V

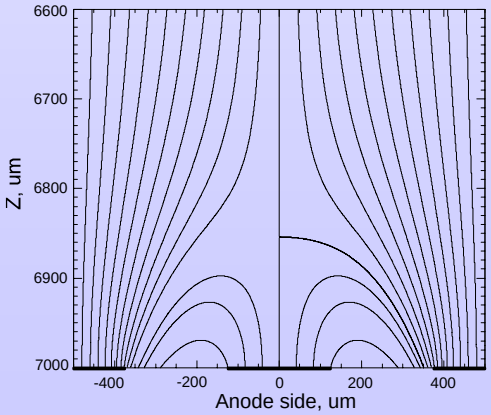

Differential bias –100V

Electric field lines near the collecting and non-collecting strips for 1000 V at the cathode and 70 V on the non-collecting grid

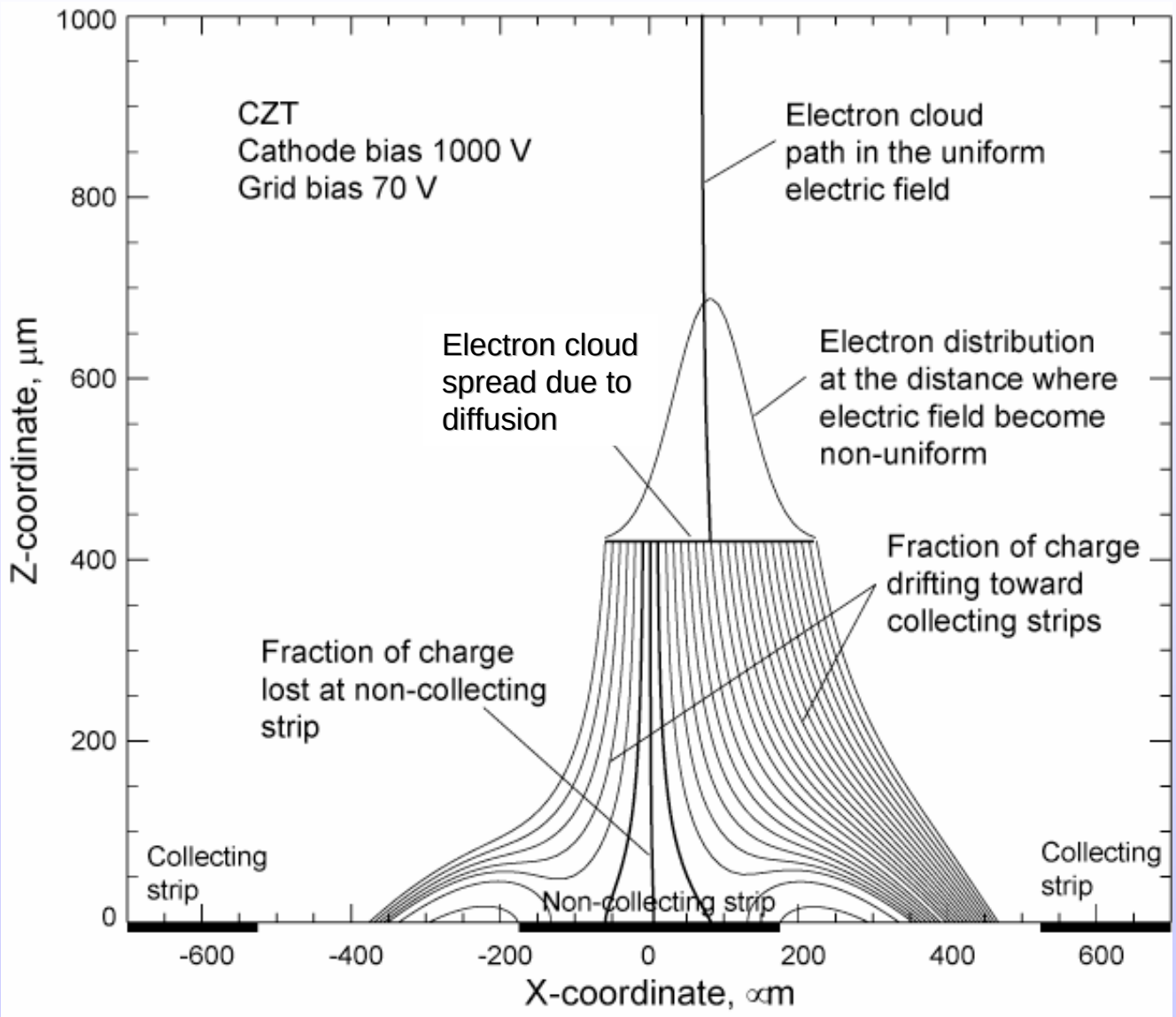

Co-planar grid studies : Conclusion

Different factors governing the performance of the co-planar grid (CPG) detectors.

❖The *global* variations, which are attributed to the asymmetry of the grids' weighting potentials, are manifested as the long tails on the right- and left-hand wings of the peaks in the pulse-height spectra.

❖The *local* variations of the device response within the pairs of adjacent strips are caused by the *local* dependence of the grids' weighting potentials and the *local* dependence of the collected charge.

Co-planar grid studies: Conclusion

These variations have not previously been considered as important. In fact, these variations, magnified by the non-uniformity of the electric field and charge loss on the surface in the gaps between the contacts, set an intrinsic limit of ~1-2% at 662 keV on the total energy resolution of current CPG detectors.

To reduce the local variations one should use grids with a larger number of thin strips. However, it may increase the grid capacities and electronic noise beyond an acceptable limit.

The origin of the electric field variations observed and the effect of surface effects need to be further investigated.

Material quality!

Outline

- Introduction: CdZnTe and gamma-ray detectors
- Frisch grid: the idea behind co-planar grid and …
- … Frisch-ring detectors
- Material defects: current limitation
- Conclusions

Frisch-ring detector

The operating principle of the device was proposed by McGregor et al., and experimentally demonstrated by Montémont et al.

Realized first at Brookhaven Lab. applying a passivation process developed by G. Wright.

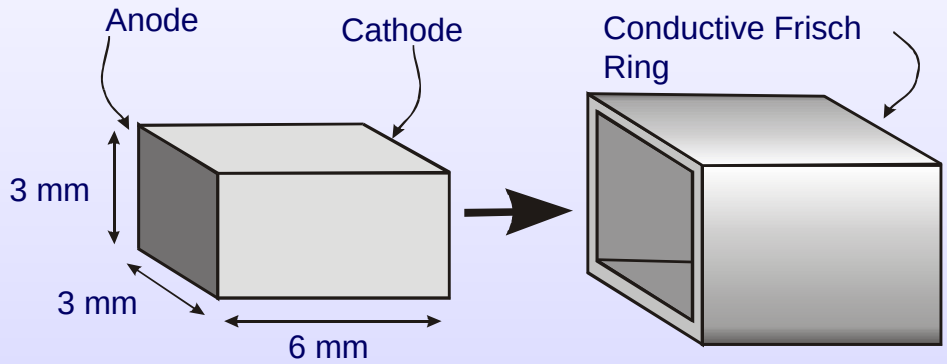

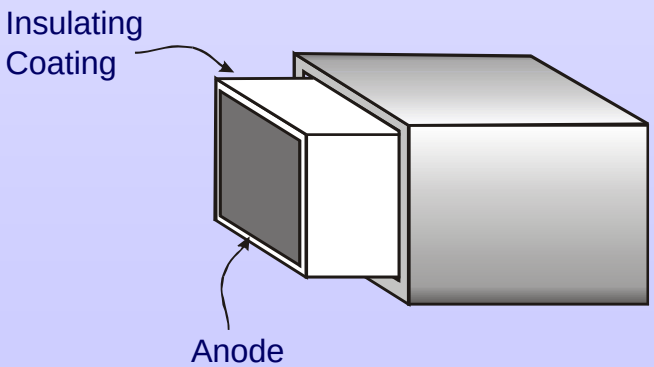

W. McNeil et al. APL **84**, No. 11, 2004

Frisch-ring detector

Advantages of bar-shaped detectors:

• made of easy-to-produce and least expensive CZT crystals (…"The invention gives scientists an inexpensive way to reproduce the high-resolution detectors -- $150 instead of $5,000." D. McGregor);

• provide good energy resolution and high stopping power due to large thickness of CZT crystals;

• can be assembled in large area arrays for imaging and spectroscopy of gamma-radiation.

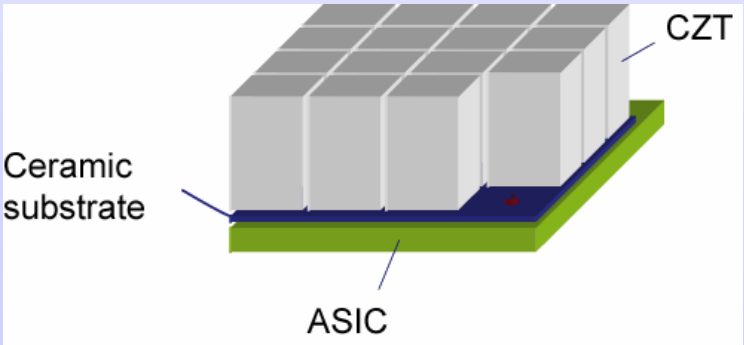

Drawback of this technique is that it is a kind of substitution of pixel device. Pixel device approach, which takes full advantage of highly expensive CZT material, is the mainstream of CZT detector developments.

Schematic of Frisch-ring detector

Single carrier device

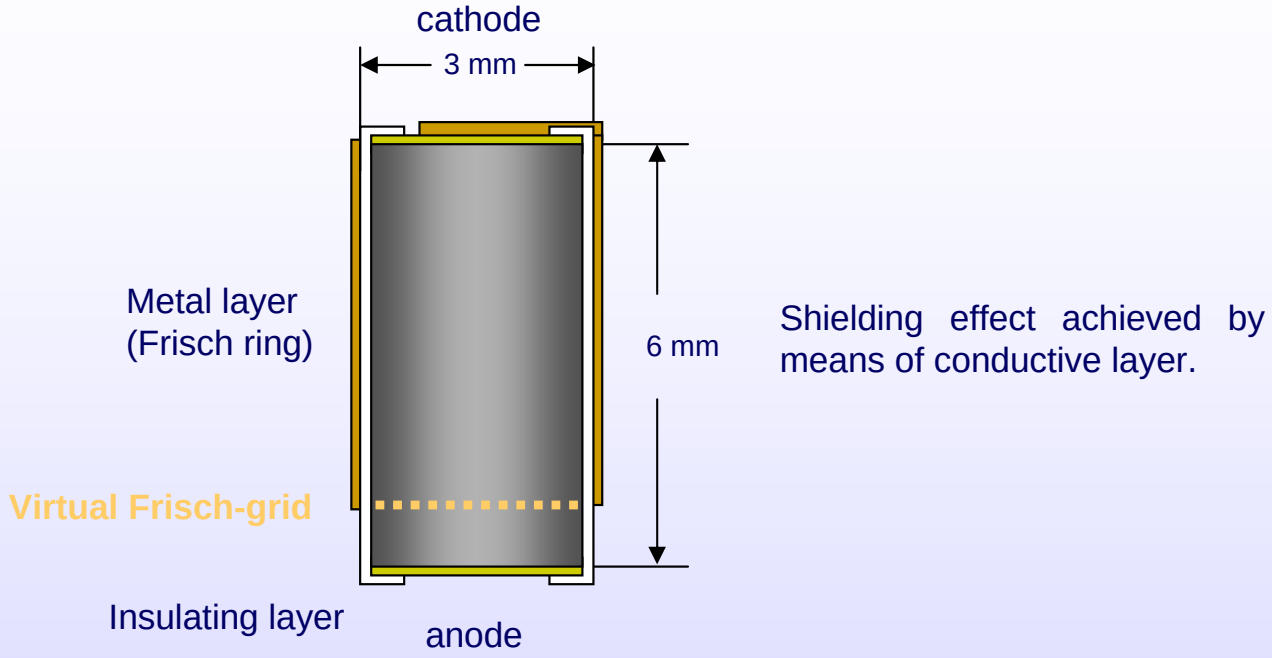

Certain geometrical aspect ratio, W/L, is required to achieve good shielding efficiency.

Screen can be modified changing: dielectric layer thickness (or permittivity value), screening depth.

Calculated dependence of the induced charge versus distance from anode

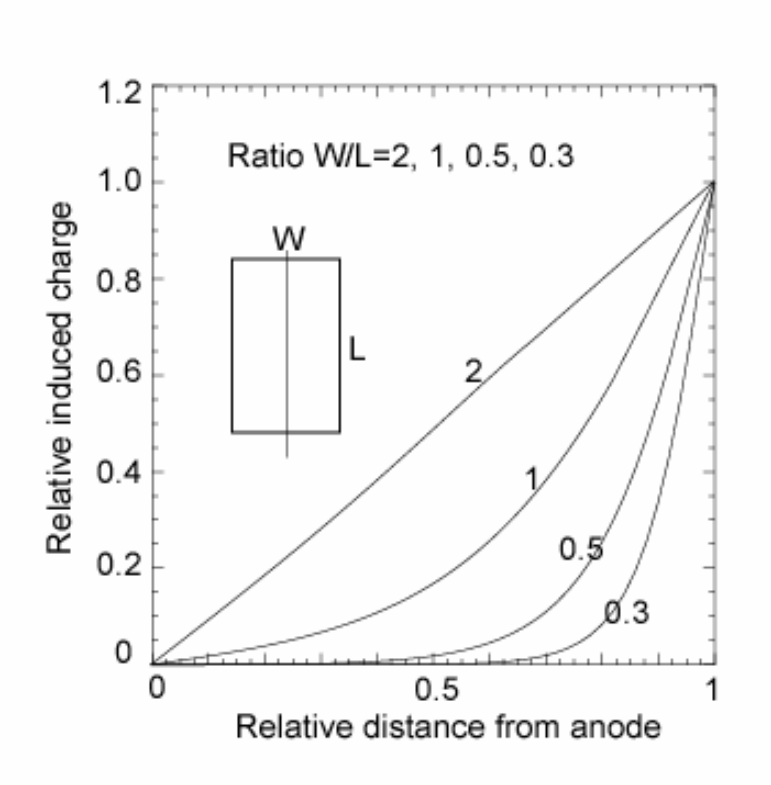

At *large aspect ratios* the dependence is linear => *planar detector*.

At *small aspect ratios* the <u>anode</u> charge is induced when the <u>source</u> charge is located close to the anode => indicates formation of *virtual Frisch grid*.

A standard solution was used for the electrostatic potential created by a point-like source charge inside the grounded metal box.

Plots were calculated for the charges located on the central axis of the box and different aspect ratios: W/L.

Simulated pulse-height spectra for several detector geometries

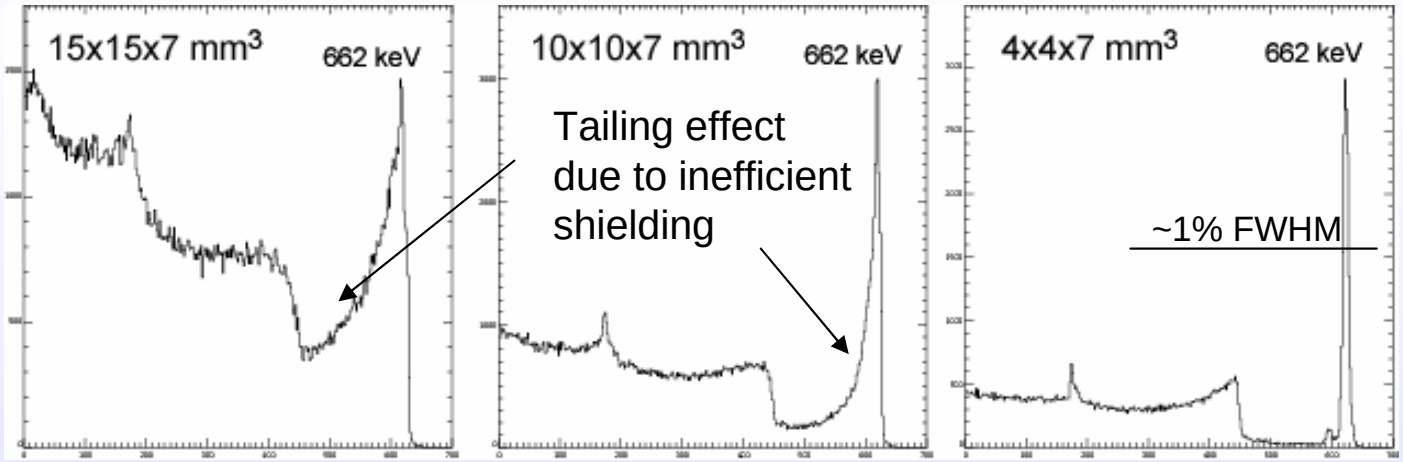

Characteristics of typical CZT crystal:

Electron $\mu\tau=5x10^{-3}$ cm^2/V
Hole $\mu\tau=5x10^{-6}$ cm^2/V

Cathode bias 1500 V
Electronic noise 2 keV FWHM

Use Monte-Carlo code to trace photons and exact solution for 3-D weighting potential to calculate charge signals.

We simulated geometry of the real experiment with the uncollimated source located on the cathode

These spectra illustrate improvements in detector response with reduction of the detector width.

For the small detector ~1% energy resolution at 662 keV and high Peak-to-Compton ratio were obtained.

This demonstrates that we can expect an excellent performance from the bar detectors with aspect ration less than 0.5.

Frisch-ring detector

For the events interacting in the measurement region, output signals depend on point of interaction which causes tailing effect.

To make this region smaller, it is desirable to have a longer detector with smaller aspect ratio.
However, there are other factors that limit thickness of the detector: maximum applied bias, electron trapping, strong electron diffusion. Optimal detector design is a trade off between all these factors.

Fabrication process

Bar-shaped CZT crystal

3x3x6 mm^3, 4x4x8 mm^3, 5x5x10 mm^3, 8x8x16 mm^3

Lapping

SiC Paper

Down to ~5 micron

Polishing

Alumina Polishing Powder on Polishing Cloth

Down to 0.05 micron Alumina Polishing Powder

Etching

2% Br_2/Methanol

Metallization

Electroless Au solution

100's nm gold film

Passivation

NH_4F/H_20_2

Detector fabrication

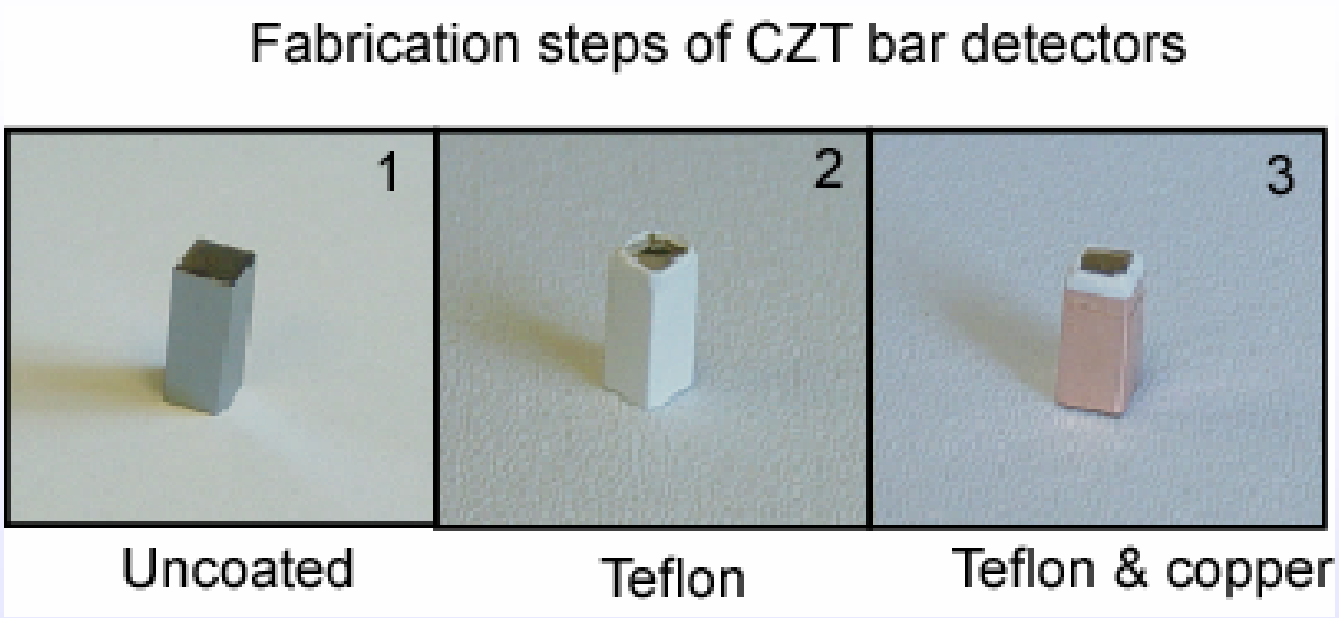

• CZT crystals are from Yinnel Tech., Inc., Saint Gobain, eV Products, and Freiburg University. Samples were re-shaped into bar detectors with different aspect ratios.

• Re-fabricate new detectors by using the same CZT crystals.

• No dependence of shield bias on detector response was observed. => Cathode and Cu shield were connected together.

• Standard spectroscopy electronics was used to collect pulse-height spectra and a digital oscilloscope to measured waveforms readout from a charge sensitive preamplifier.

• In the beginning of the project, significant variations were observed in the measured pulse-height spectra. From excellent to very bad.

• Later we learn how to fabricate good devices with ~100% yield!

Experimental setup

Bar detector inside eV Products holder

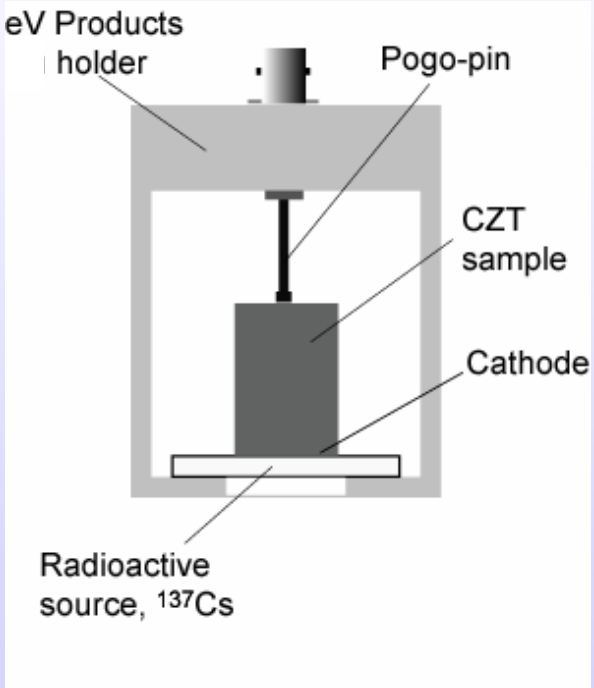

Source located inside the holder to ensure that photons enter detector from cathode side.

Resolution vs Ring Length

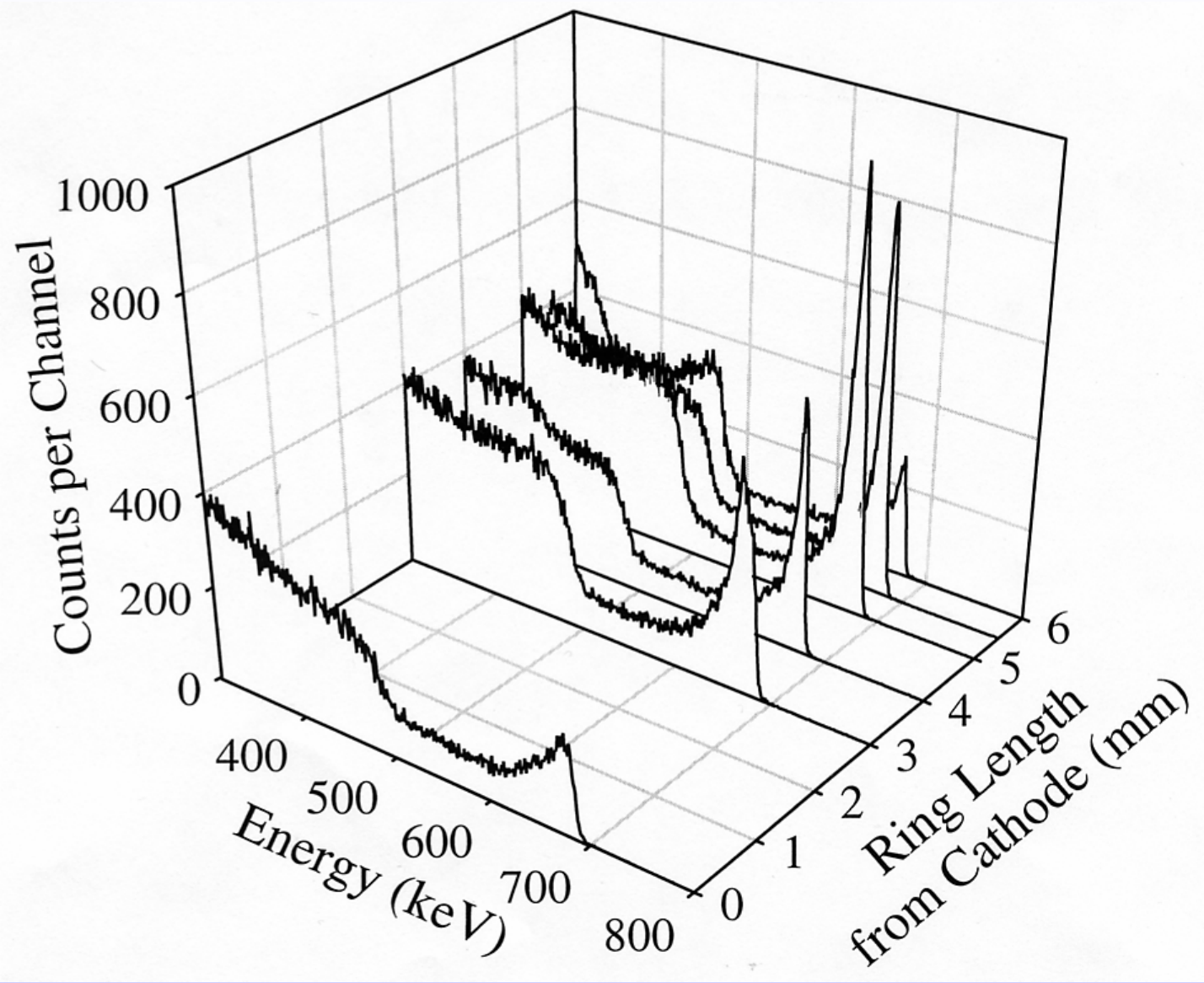

W. McNeil et al. APL **84**, No. 11, 2004

Shielded / not shielded

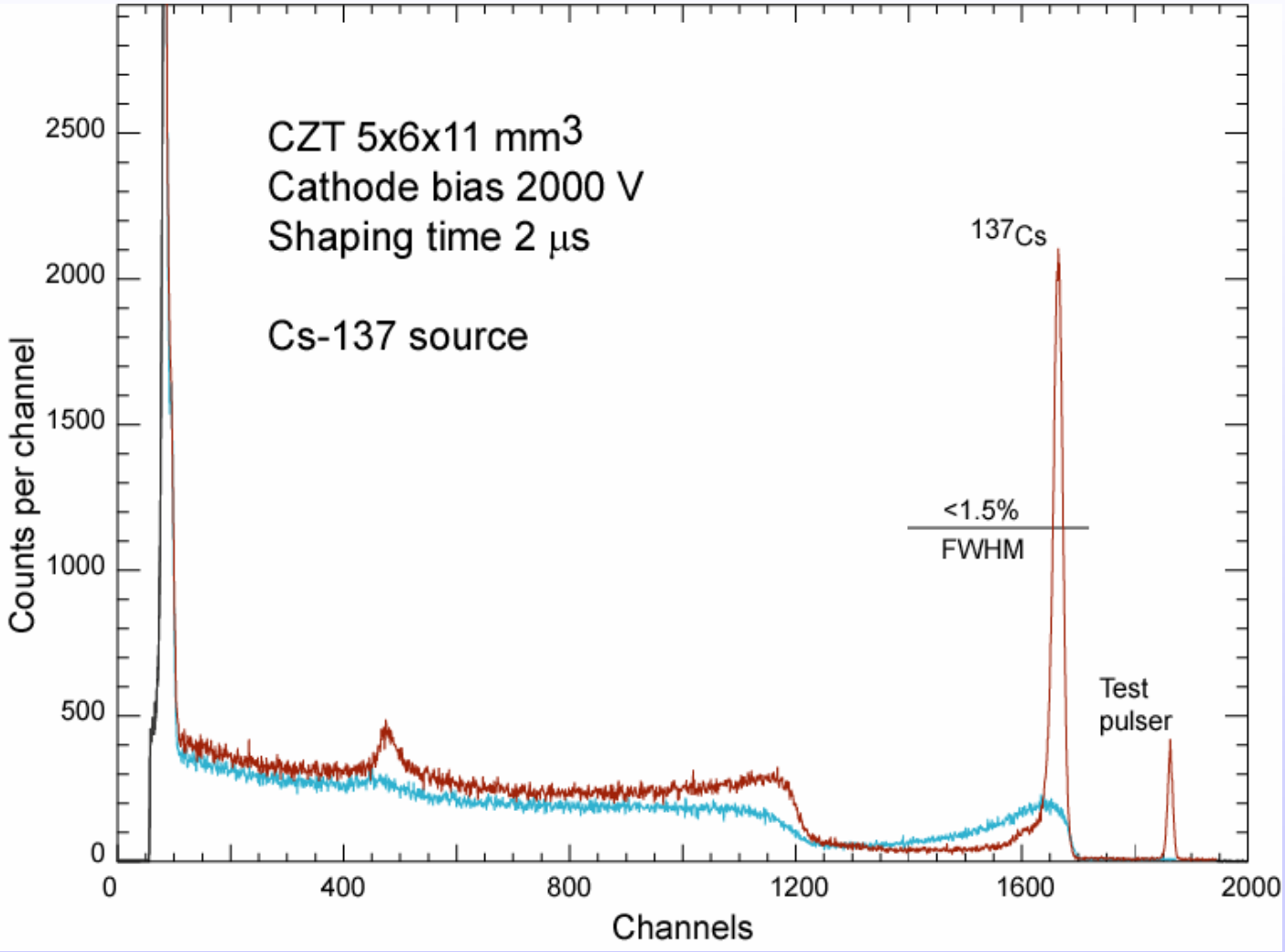

Improvement of detector response after chemical treatment of the side surfaces

Detector performance depends on the surface quality and surface passivation.

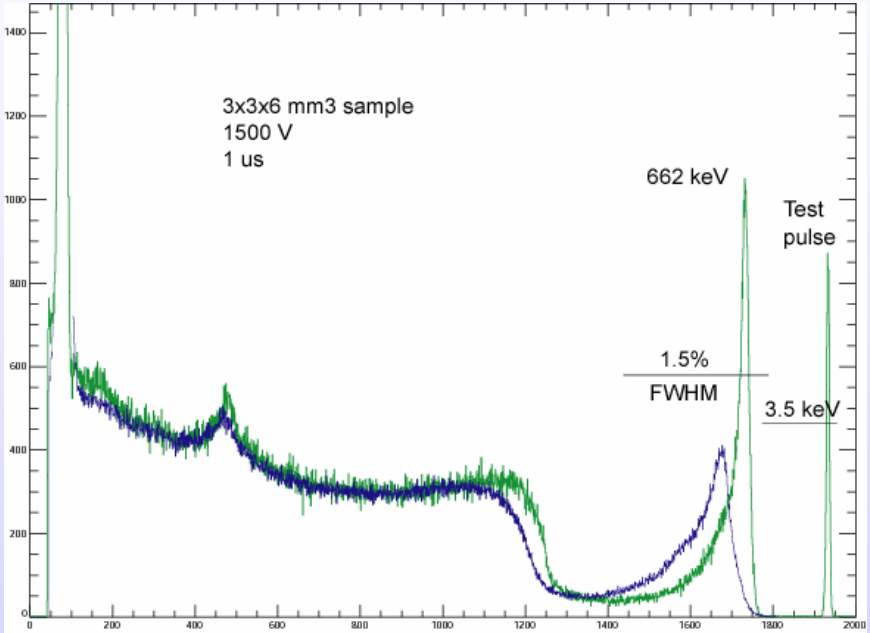

Improvement of the detector response after surface treatment with NH_4F/H_2O_2 (ammonium fluoride) solution (proposed by G. Wright).

The field lines distribution is determined by the boundary conditions on side surfaces which depends on surface resistivity.

Examples of pulse-height spectra measured with detectors …

Satellite peaks, strong tailing, and low-energy background are very common features in the spectra from the “bad” detectors.

We found, that detectors re-fabricated from the same crystals had different responses. This suggests that internal crystal defects cannot completely explain poor detector responses.

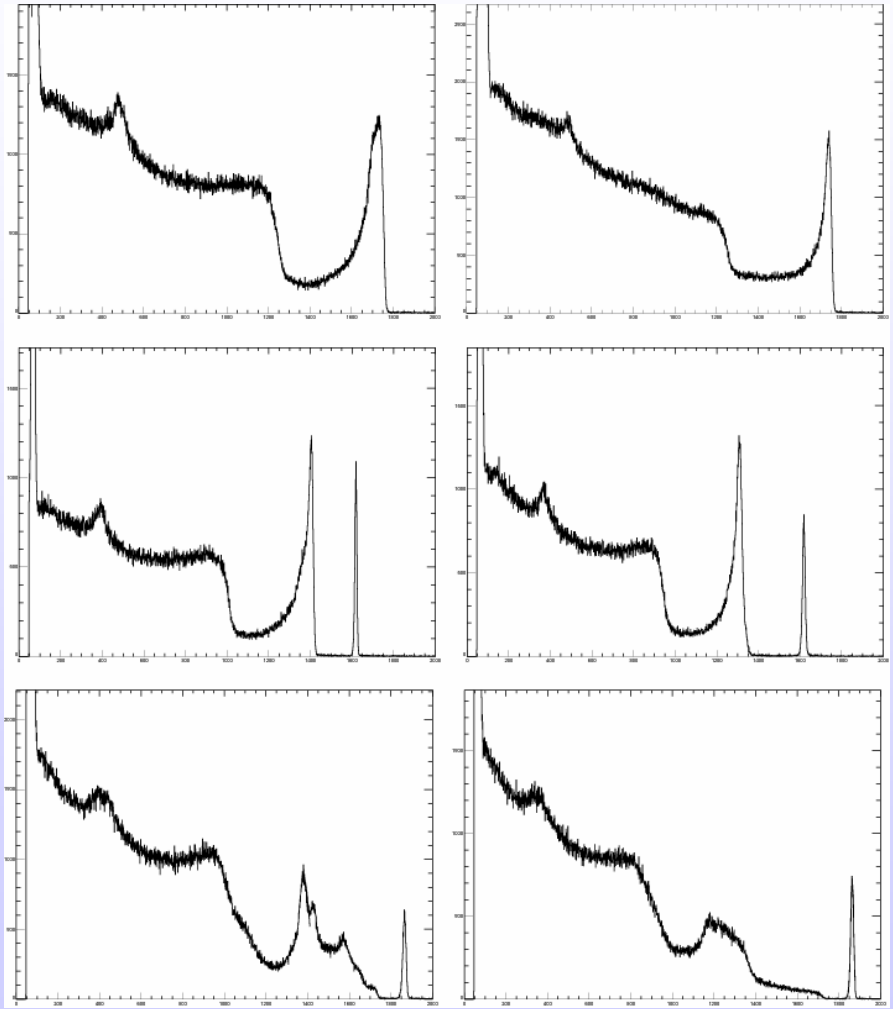

5x5x7 mm3

4x4x7 mm3

4x4x7 mm3

…that had poor performance

Examples of pulse-height spectra measured with detectors …

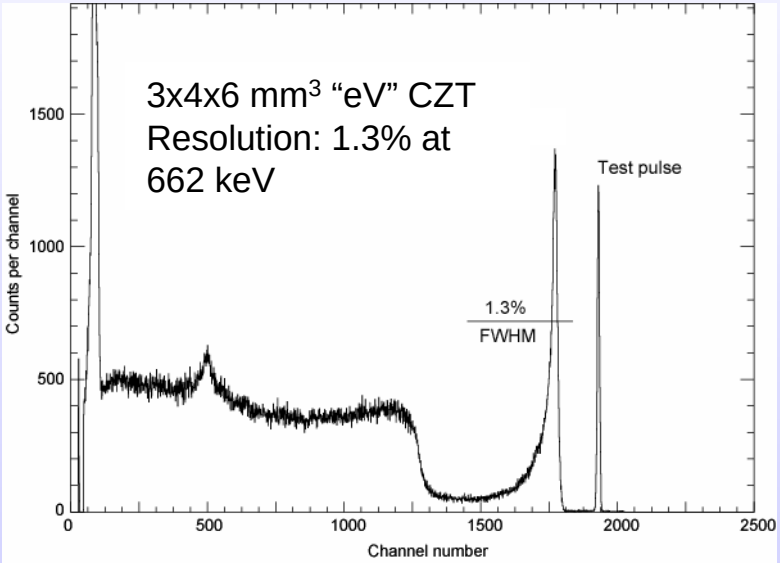

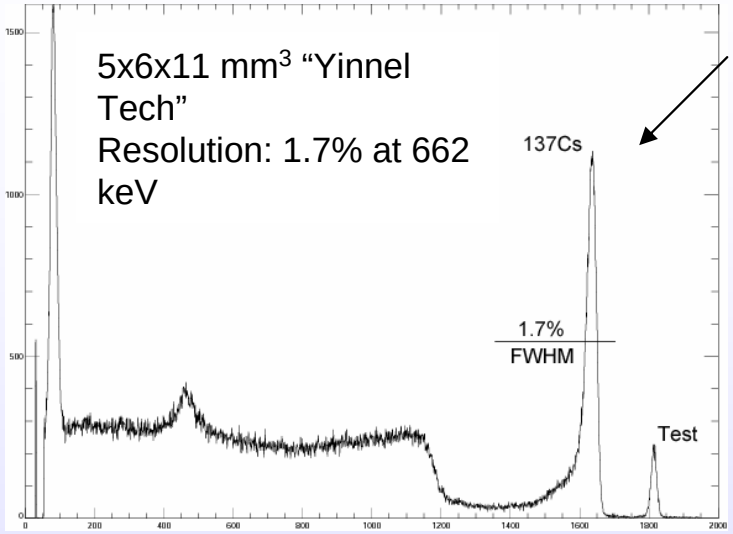

We expected better result

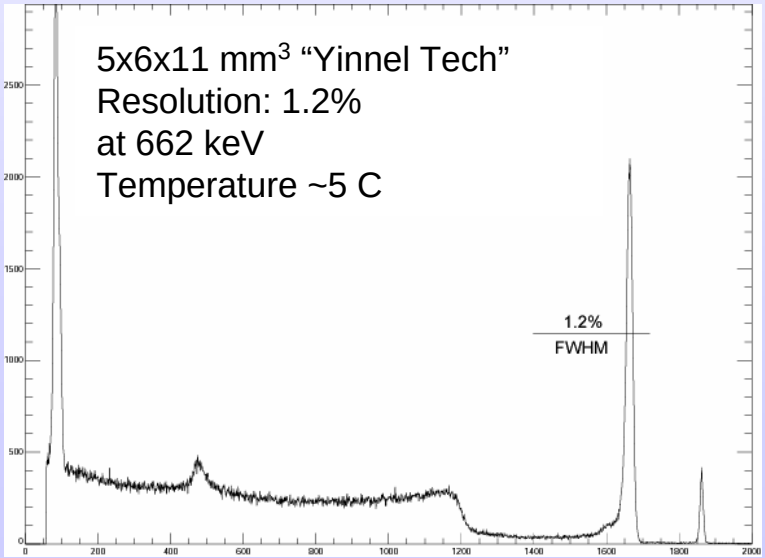

…that had good performance

Good 5x6x11 mm3 detector

5x6x11 mm^3 “Yinnel Tech
at room temperature

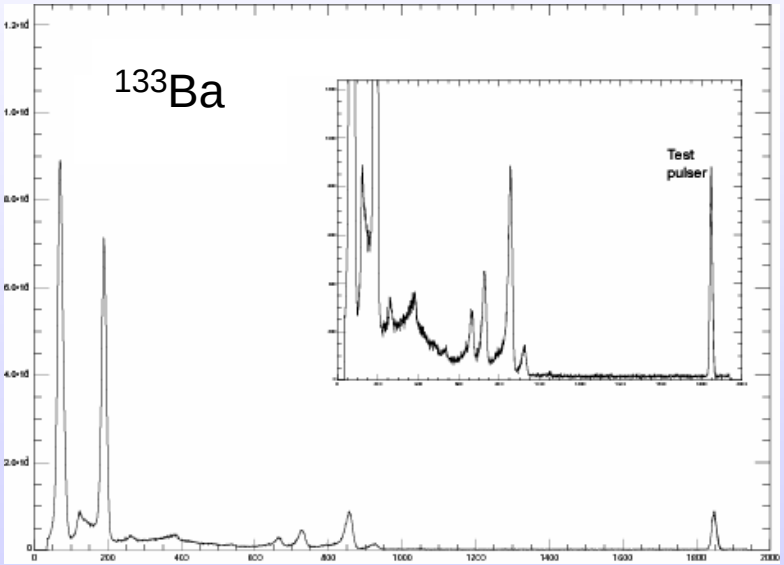

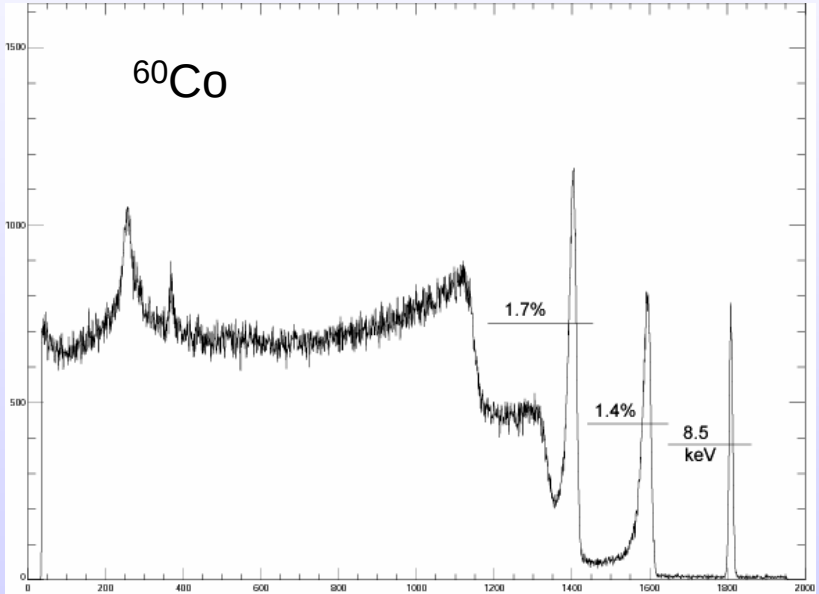

Frisch-ring detector : summary

- Frisch-ring detectors have many potentials.

They provide: good energy resolution, <1.5% FWHM at 662 keV and high stopping power

- To fabricate “good” detectors it is important:

(1) shield entire area of side surfaces,

(2) use thin insulating layer,

(3) use CZT crystals with small aspect ratio, <0.5

(4) ensure a “focusing” field inside the device

An extensive waveforms analysis support these assumptions.
De-focusing field is the main factor that degrades the response of bar detectors.
Solution: correct surface preparation and passivation.
Unfortunately, there are other effects degrading the device response.

Frisch –ring detector: X-ray scans

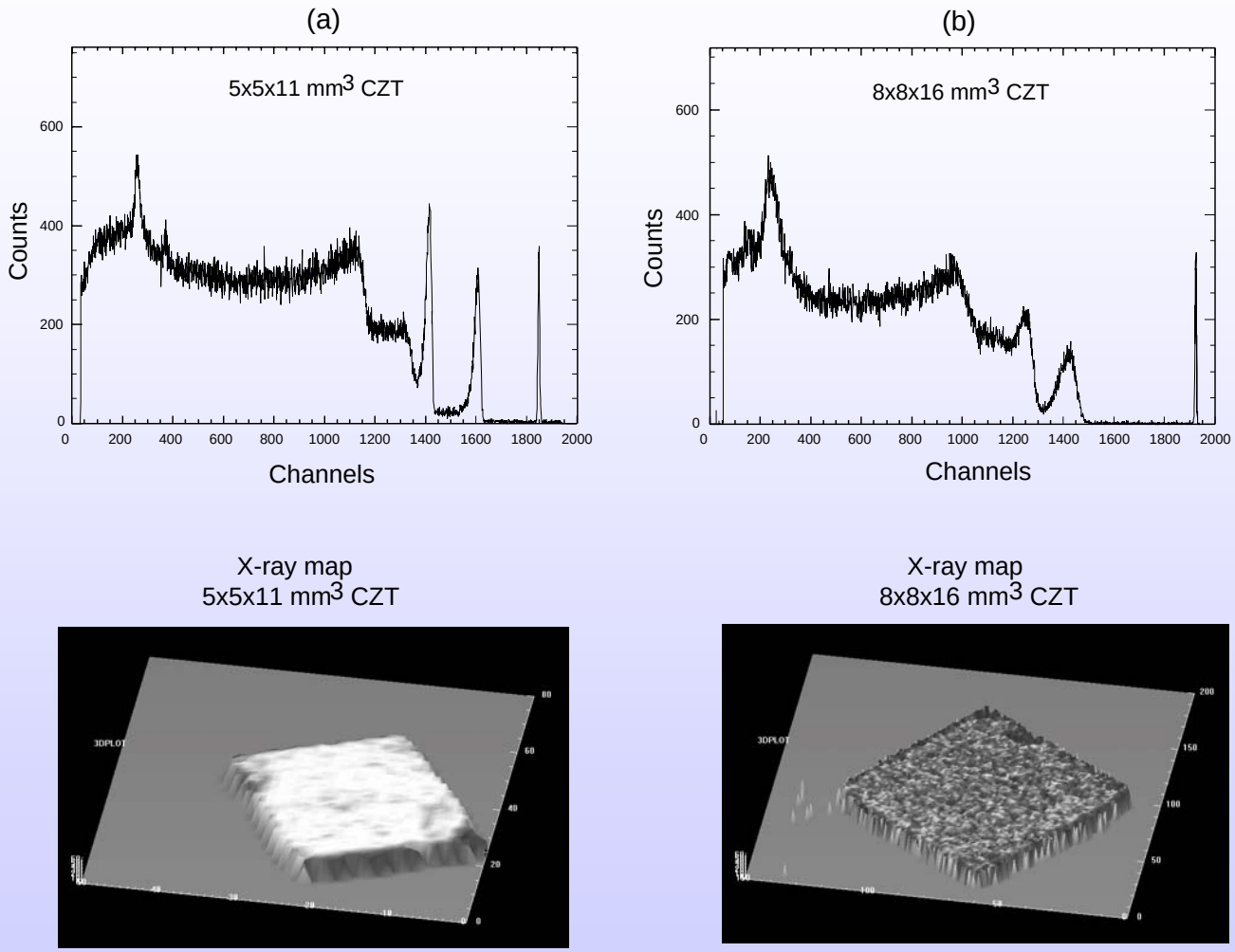

The starting point of this study was the observation of poor spectroscopic performance and non uniform gamma response in virtual Frisch grid CZT detectors.

Setup

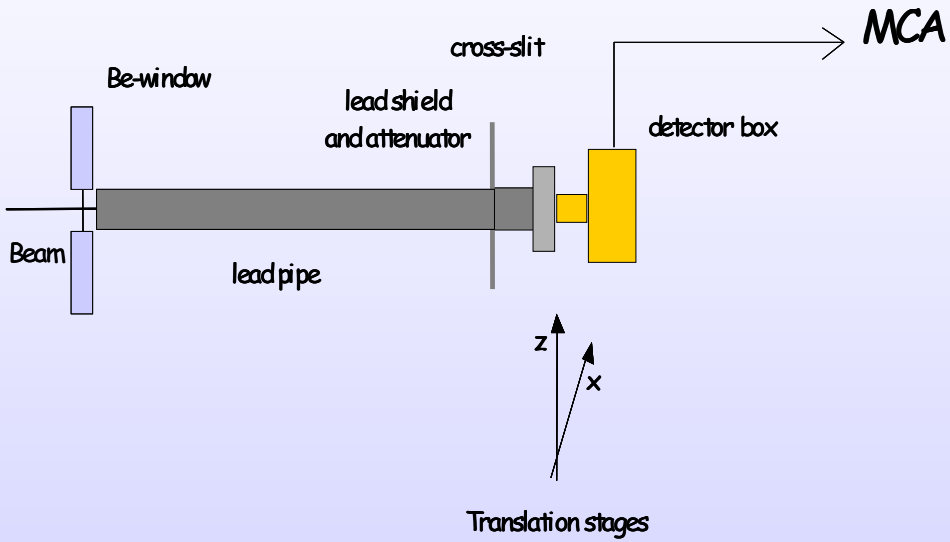
MCA
cross-slit
Be-window
lead shield
and attenuator
detector box
Beam
lead pipe
z
x
Translation stages

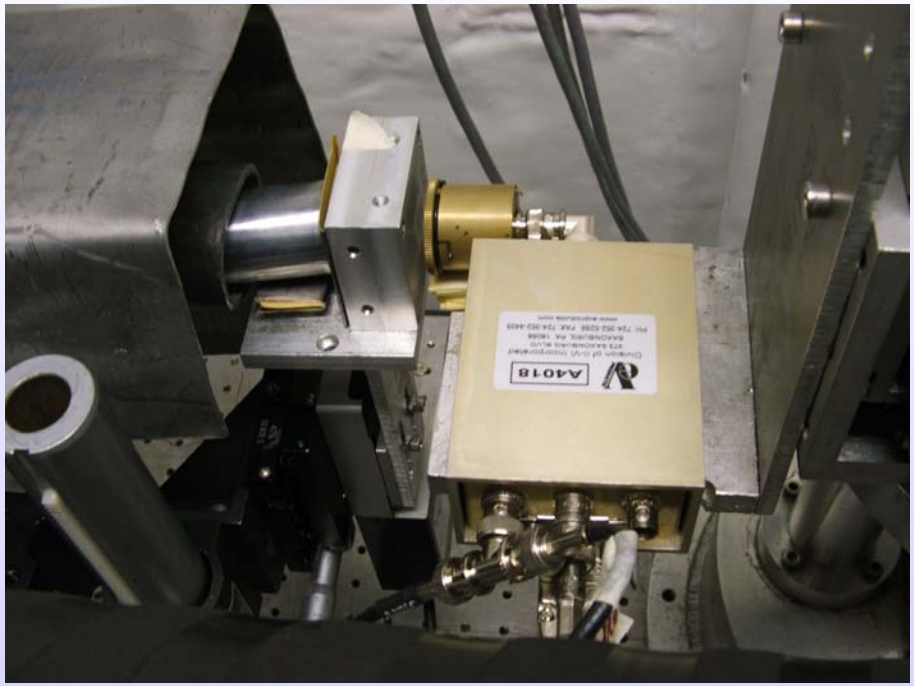

Setup parameters

Two different operation modes :

white beam mode with attenuator - 85keV (FWHM 10keV)

monochromatic mode - 30keV beam energy.

The absorption length in the first case is up to 3mm. That is the situation for which the sample is uniformly irradiated.

In the second mode the absorption length is 10 times less (~ 300μm). In this case the charges are mostly created in the first layers of the crystal and then they propagate to the anode.

No difference, from the correlation point of view, resulted between the two operation modes.

Beam size = 10μm x 10μm
Step size = 10μm
Crystals size = 5 x 4 x 1.2 mm^3
V_B = 50V
Time of collection per point = 1.5s
Shaping time = 0.5μs

Gamma map of a thin crystal

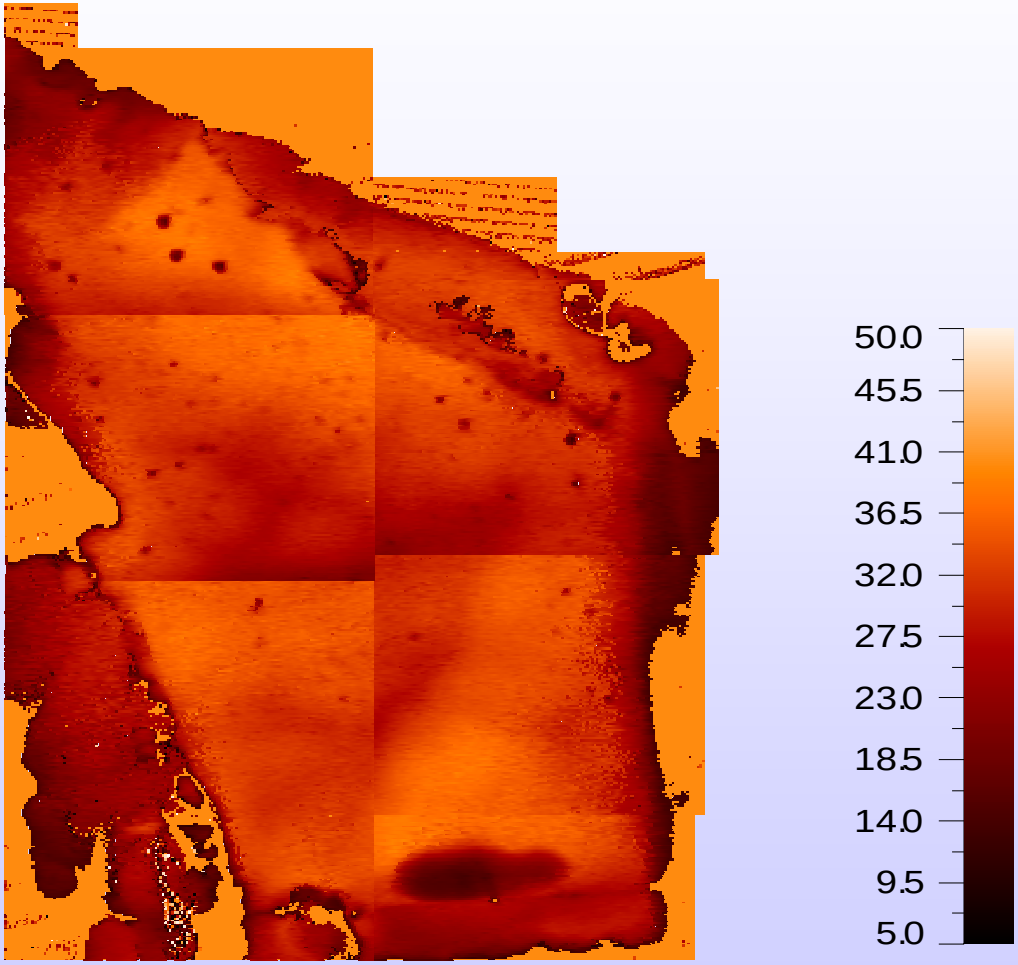

Maps Correlation

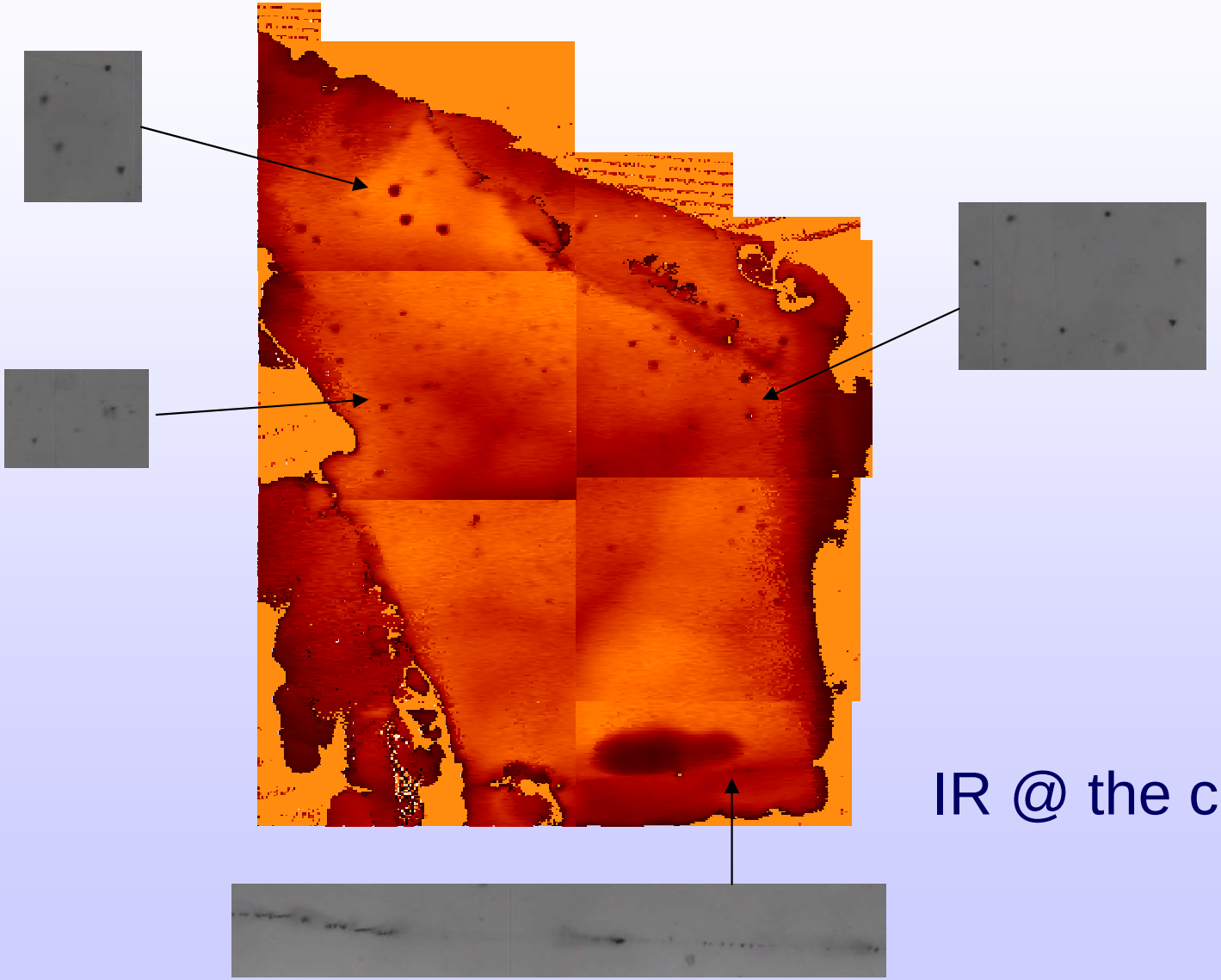

IR @ the cathode

Maps Correlation

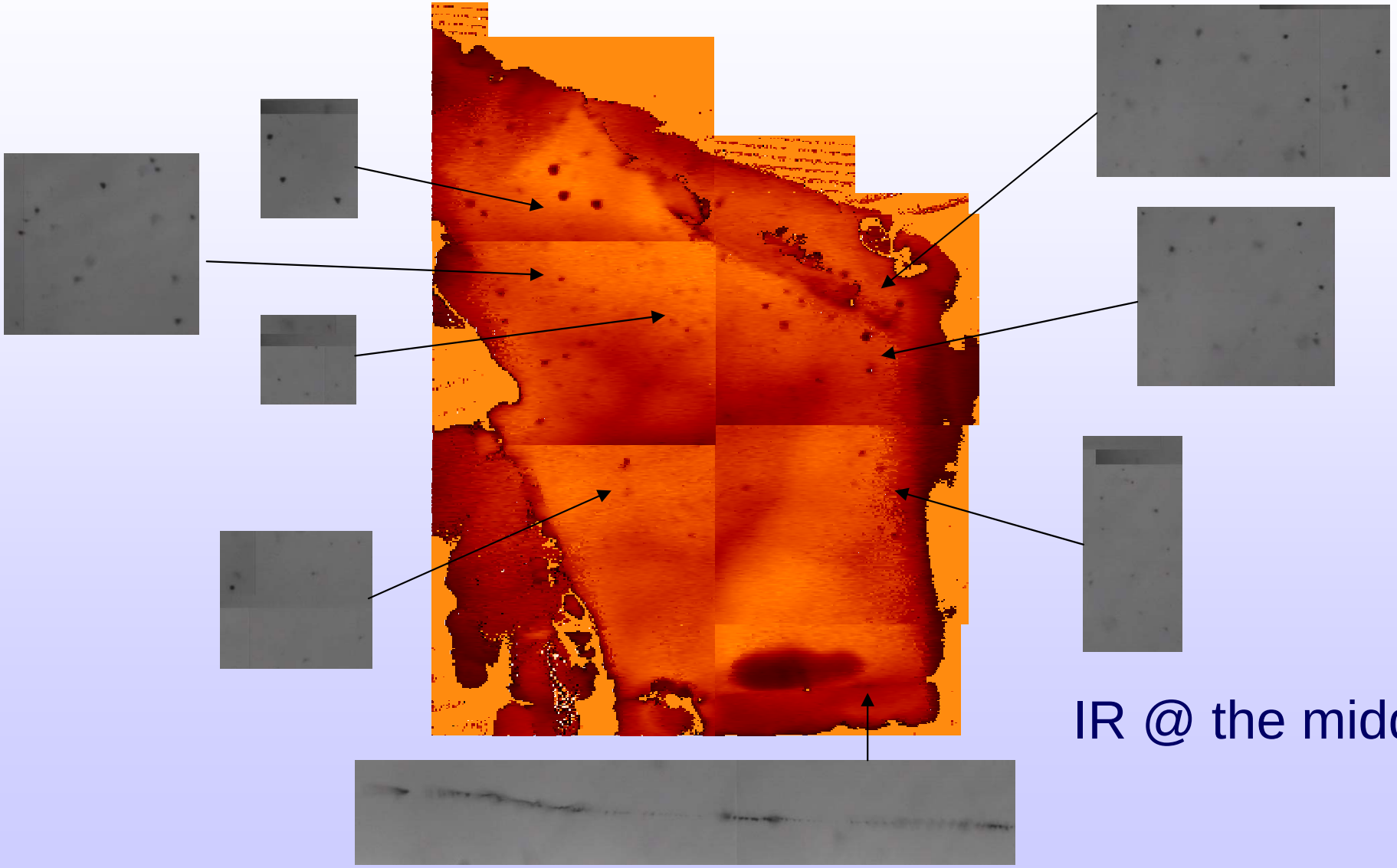

IR @ the middle

Maps Correlation

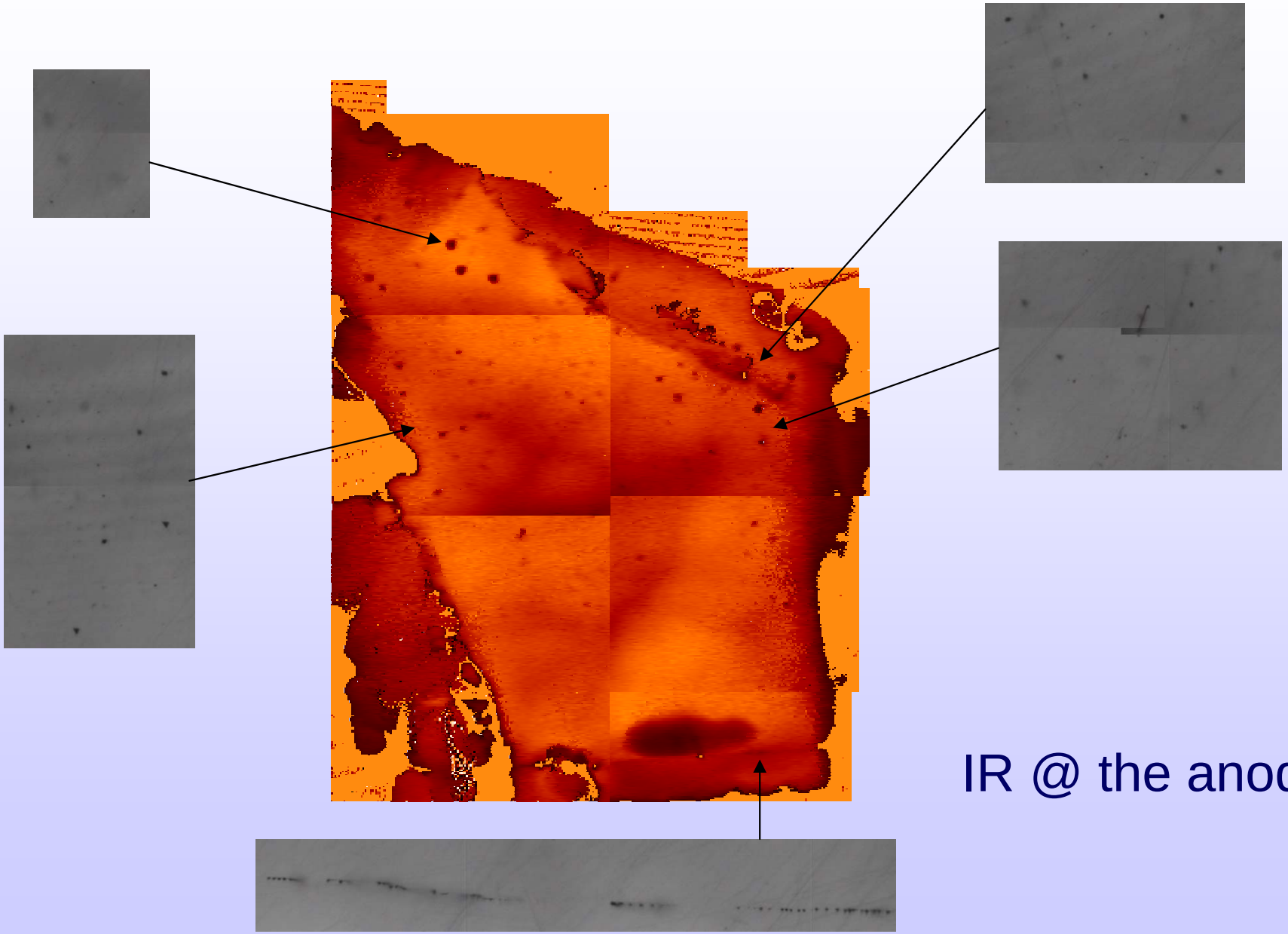

IR @ the anode

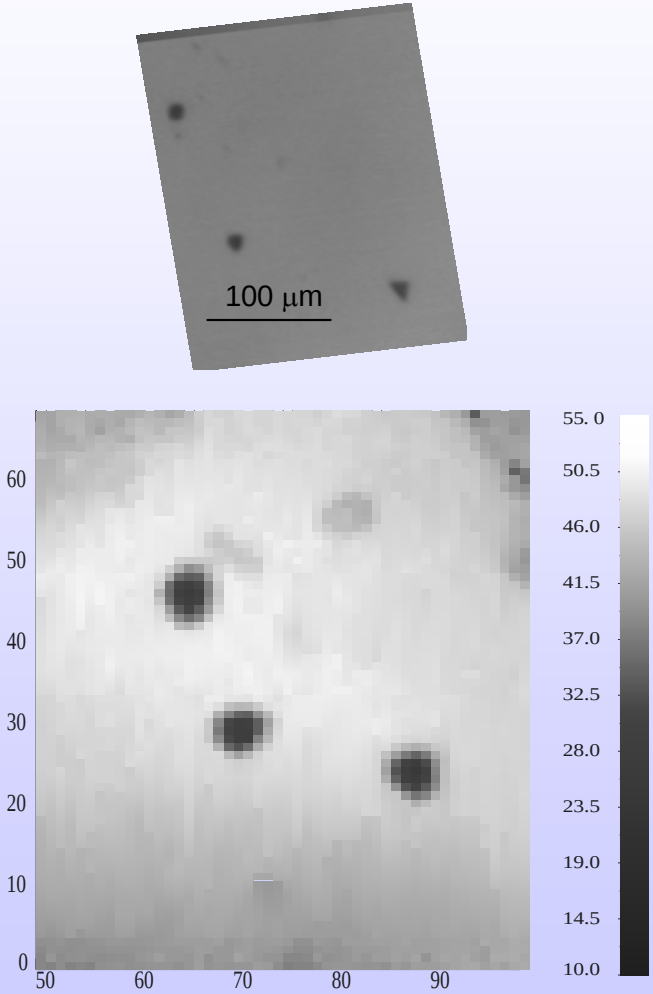
100 μm
60
50
40
30
20
10
0
50
60
70
80
90
55. 0
50.5
46.0
41.5
37.0
32.5
28.0
23.5
19.0
14.5
10.0

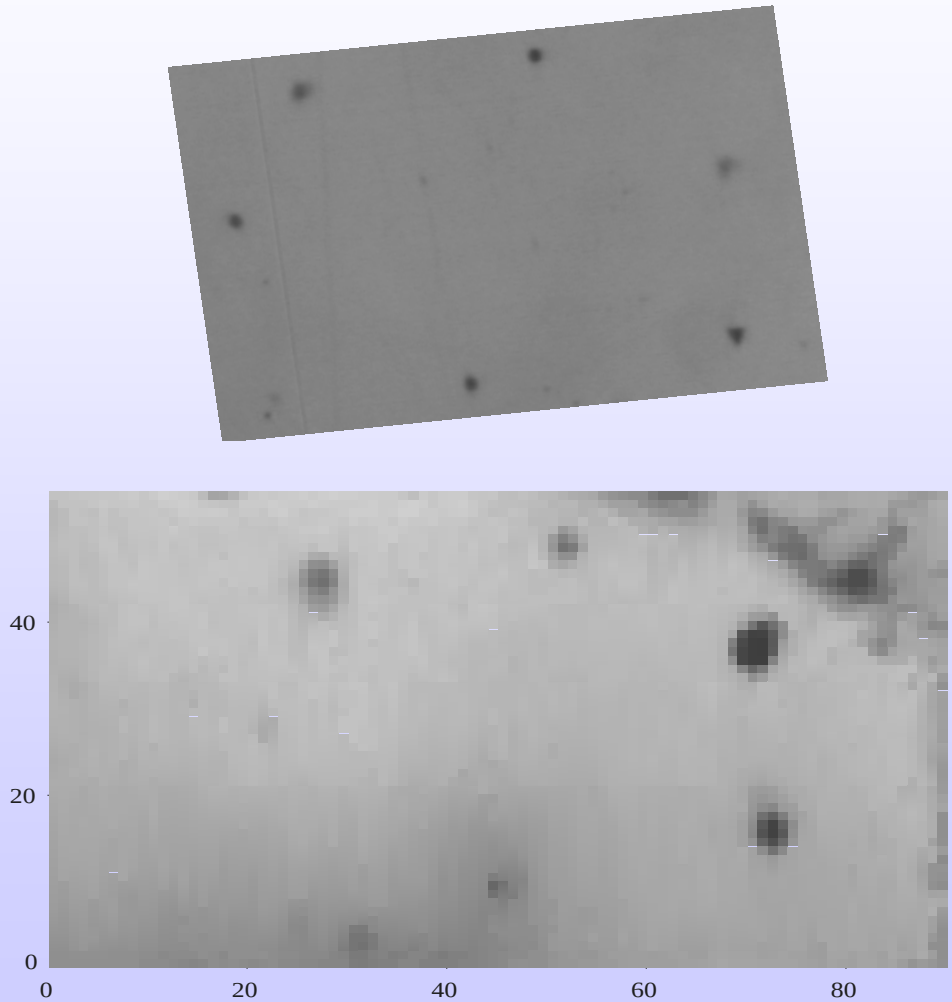
40
20
0
0
20
40
60
80

Some Spectra

Average values
p.p. = 32, FWHM = 12

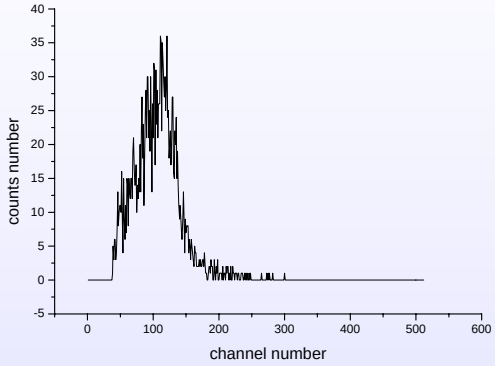

p.p. = 20.9, FWHM = 12.2

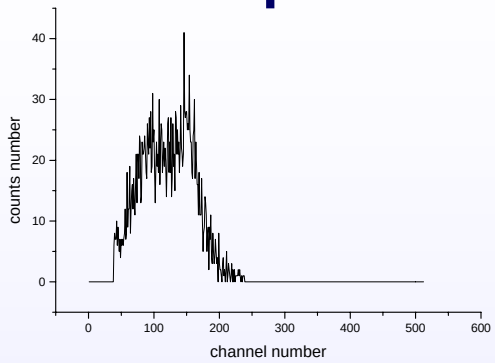

p.p. = 17.2, FWHM = 18.7

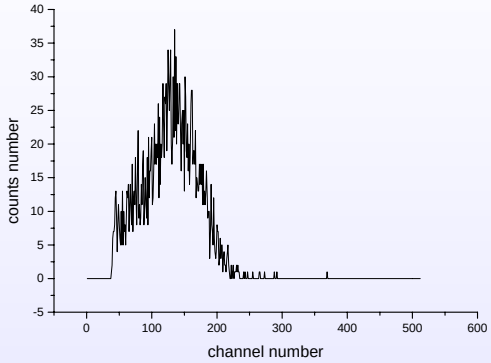

p.p. = 26.4, FWHM = 18.1

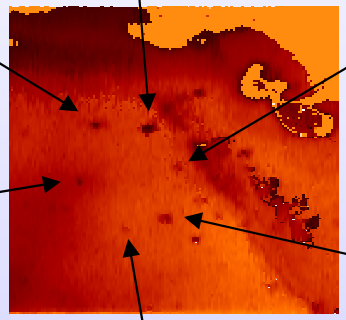

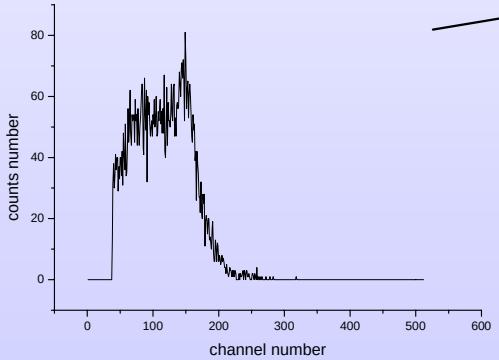

p.p. = 21.7, FWHM = 26.2

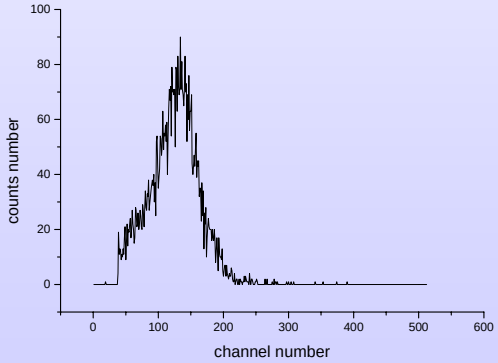

p.p. = 25.8, FWHM = 12.7

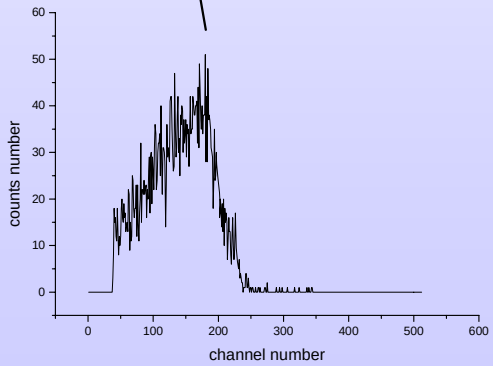

p.p. = 28.8, FWHM = 23.2

…from 25 μm to 10 μm

White beam mode with attenuator
Crystal size = 5 x 5 x 2.1 mm^3
Time of collection per point = 2s

Beam energy ~ 85 keV
V_B = 70V
Shaping time = 0.5μs

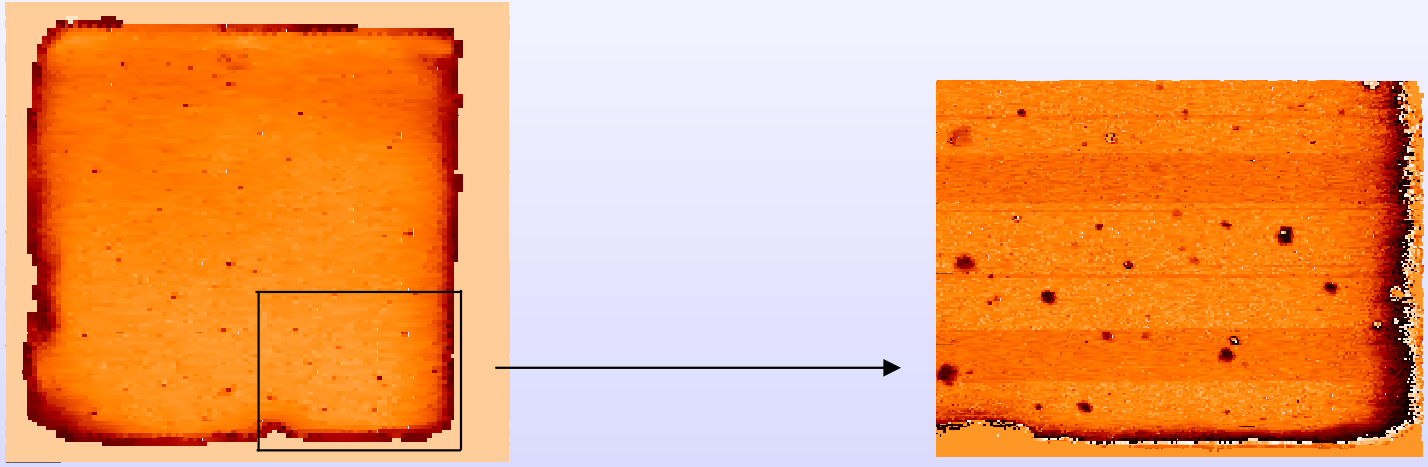

Beamsize 25 μm x 25 μm
Step 50 μm

Beamsize 10 μm x 10 μm
Step 10 μm

Beam energy ~ 30 keV
Time of collection per point = 1s

V_B = 50V
Shaping time = 1μs

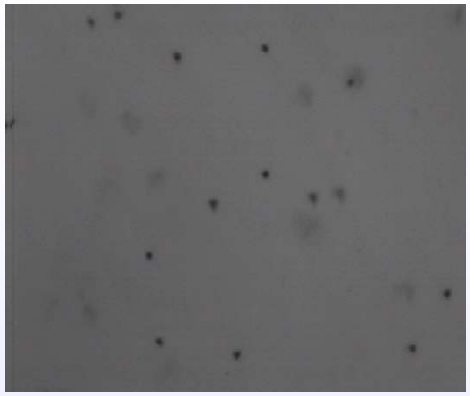

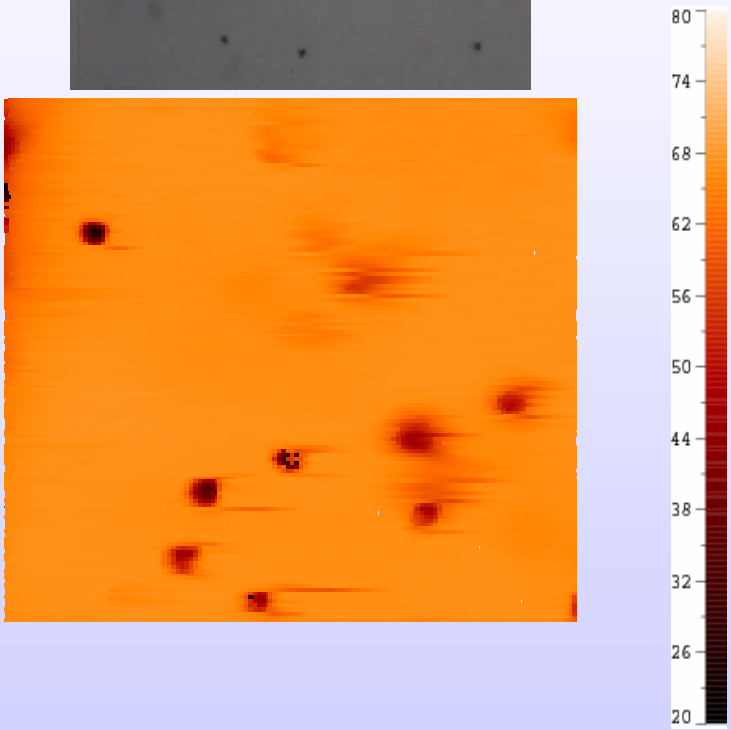

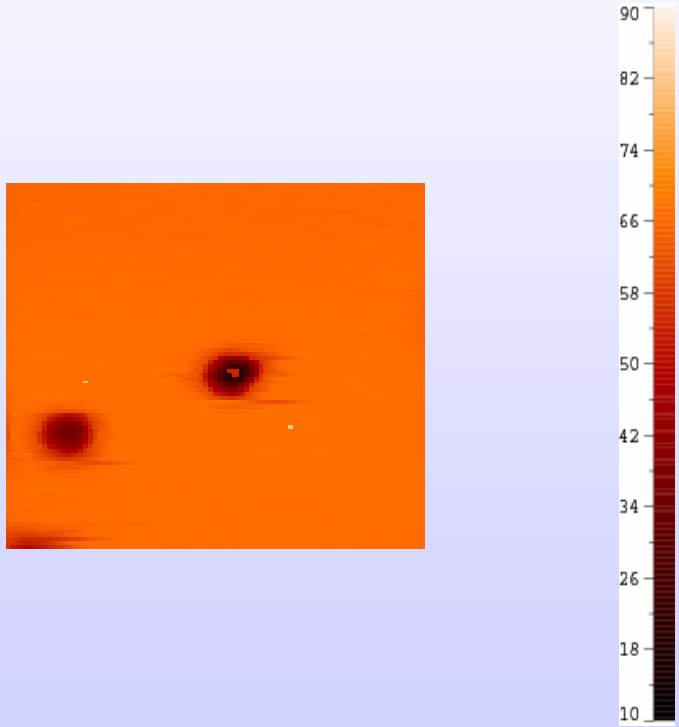

Step 6μm

Step 3μm

0.8 x 0.8 mm^2

0.3 x 0.3 mm^2

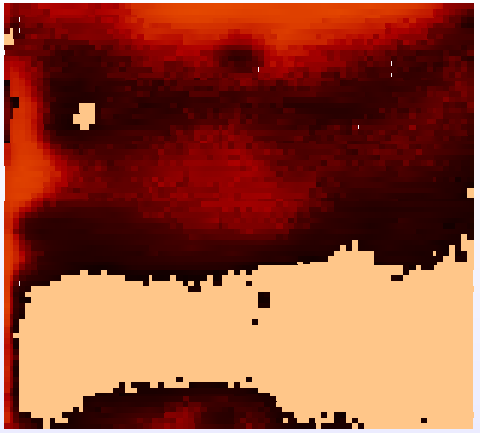

20V

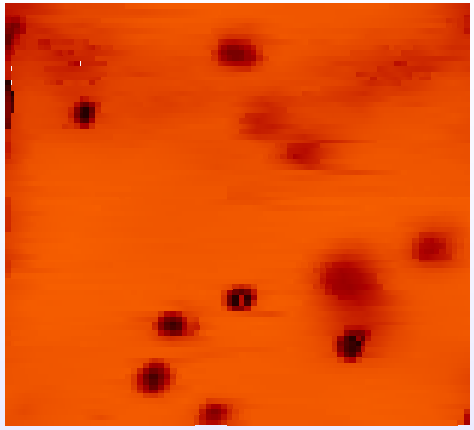

25V

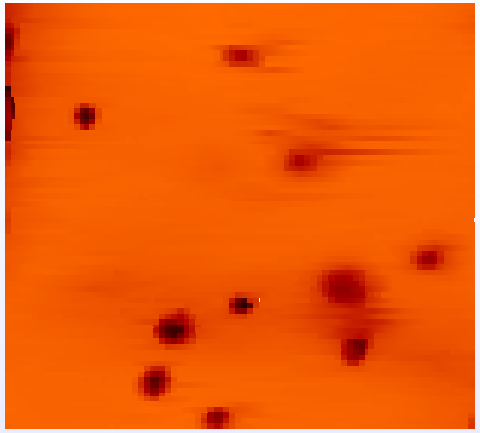

35V

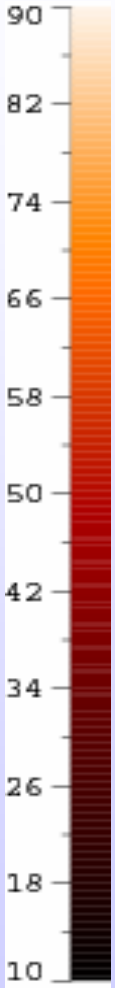

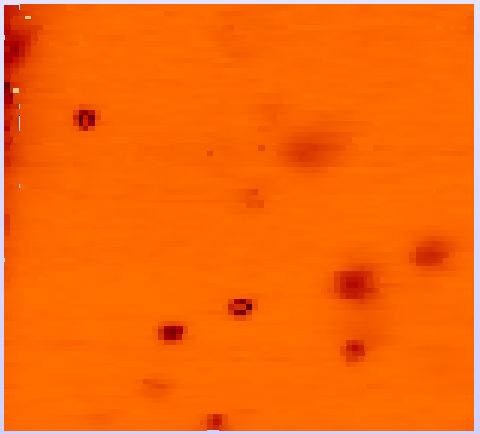

60V

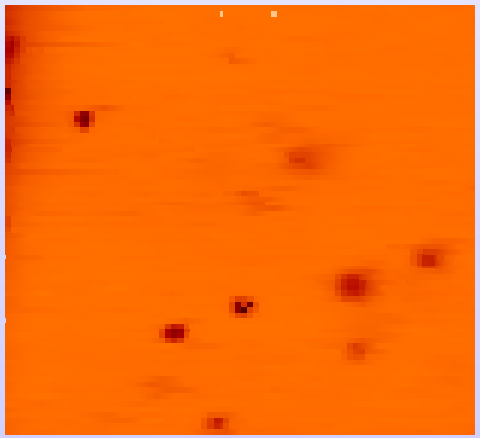

75V

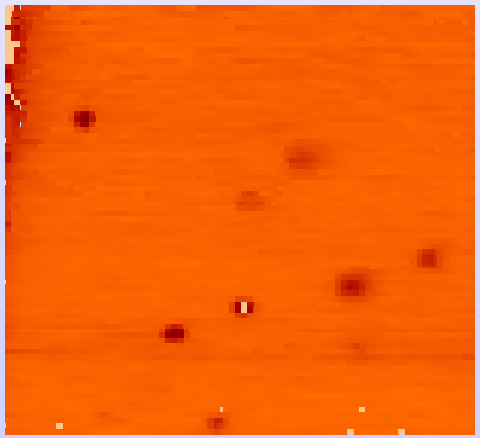

90V

0.8 x 0.8 mm^2

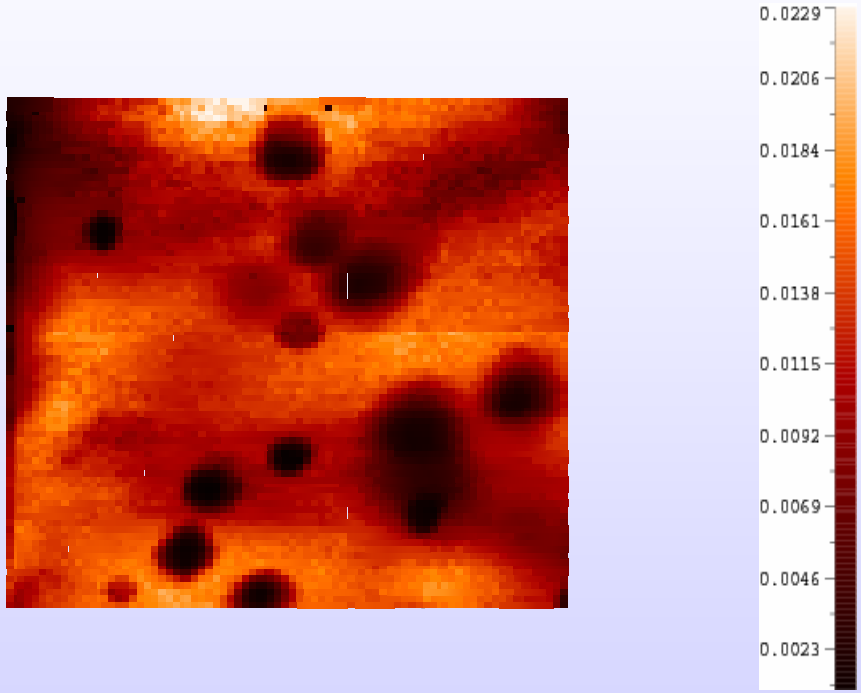

$\mu_e\tau_e$ map

Hecht relation $Q=Q_0(\mu\tau E/d)(1\text{-}\exp[-d/\mu\tau E])\}$

Simulated maps for: a) 400 x 400 μm^2 beam / 400 μm step size; b) 200 x 200 μm^2 beam / 200 μm step size; c) 100 x 100 μm^2 beam / 100 μm step size; d) 50 x 50 μm^2 beam / 50 μm step size; e) 20 x 20 μm^2 beam / 20 μm step size. f) 2D maps from a scan performed by using a 30 keV beam, shaped with a 10 x 10 μm^2 double slit and a 10 μm step size.

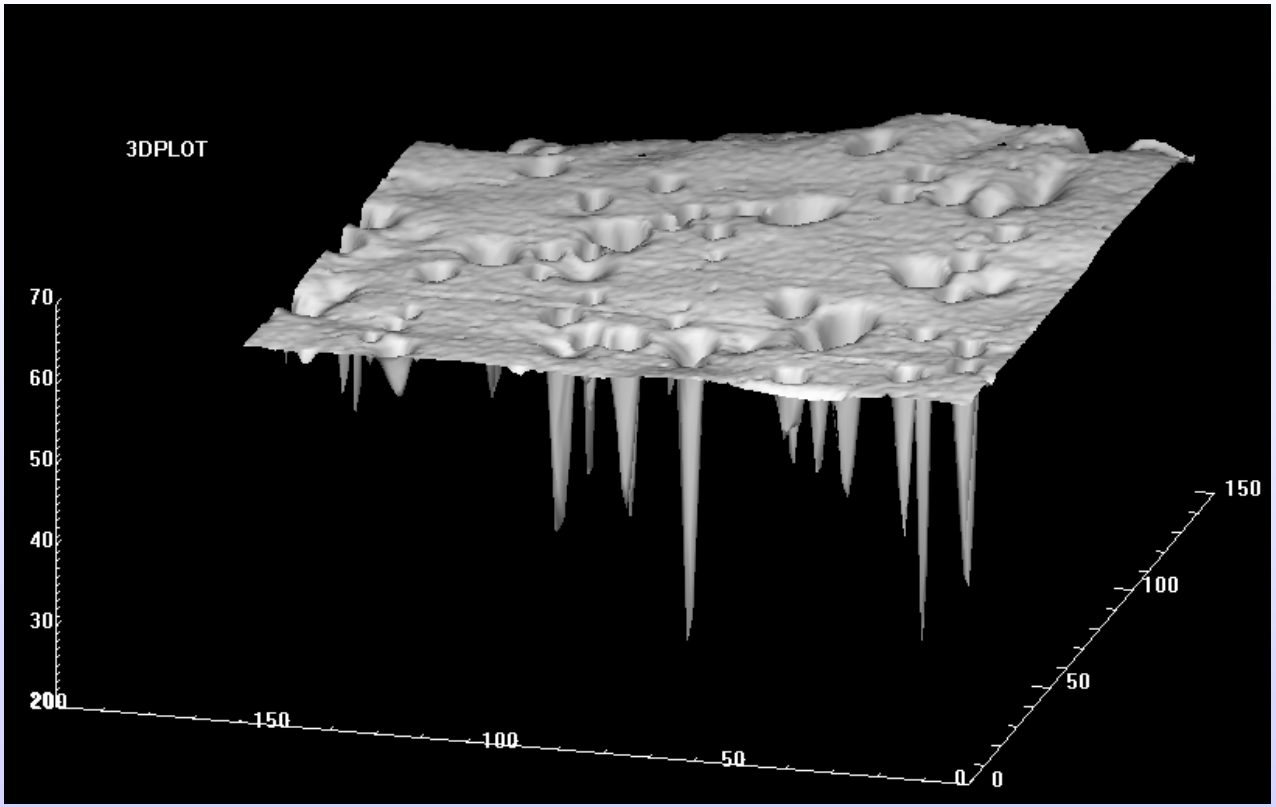
3DPLOT
70
60
50
40
30
200
150
100
50
0
0
50
100
150

Conclusions

It's known that…

- Non uniform trapping and non uniform electric field distribution cause charge transport non uniformity.

- Structural defects: they cause charge trapping and recombination.

- Strong trapping yields to a space charge region that effects the electric field.

We have shown the effects of Te inclusions in the charge collection and ultimately in detector performances.

Conclusions

Future

CPG → Surface effect studies on detector with different surface processes

Frisch-ring → Design and surface treatment improvement
Array detectors development

Material → Continue characterization with better resolution

Acknowledgements

Z. Yin, W. Caliebe, J. Jakoncic

T. Lenhard, R. Green, T. Kuczewski, D. Poshka

P. O'Connor, G. Smith, V. Radeka

J. Triolo, D. Pinelli

P. Vanier, C. Czajkowski, Joe Indusi

C. Arnone